NRIAG Journal of Astronomy and Geophysics (2016) 5, 124–146

National Research Institute of Astronomy and Geophysics

NRIAG Journal of Astronomy and Geophysics

www.elsevier.com/locate/nrjag

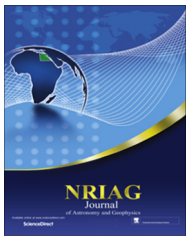

Hydrogeological, petrophysical and hydrogeochemical characteristics of the groundwater aquifers east of Wadi El-Natrun, Egypt

Zenhom E. Salem [a,*], **Dina A. El-Bayumy** [b]

[a] *Geology Department, Faculty of Science, Tanta University, Tanta, Egypt*
[b] *Ministry of Water Resources and Irrigation, Egypt*

Received 4 February 2015; revised 8 October 2015; accepted 30 December 2015
Available online 4 February 2016

KEYWORDS

West Nile Delta;
Wadi El-Natrun;
Sadat City;
Groundwater;
Aquifer petrophysics;
Hydrogeochemistry;
Groundwater depletion and level rise

Abstract The studied water-bearing formations in the investigated area are the Quaternary and the Miocene aquifers. The groundwater movement takes a direction from the eastern and northern directions where the surface water sources are located to the western and southern directions. By comparing the water level data of 1960 and 2010, up to 25 m drawdown was noticed in the southern part due to excessive pumping. On the other hand, water level rising was observed in the same period reaching up to 10 m in the northwestern part due to seepage from the irrigation channel.

Petrophysical properties of the studied aquifers were estimated from well logs. The formation water resistivity (R_w) averages 15.2 ohm m whereas the formation factor (F) averages 5.1. The averages of the total porosity, the effective porosity and permeability are 36.5%, 33.1% and 1126.3 mdarcy, respectively. In addition, the gamma ray logs were used to estimate the volume share of shale which showed an average value reached about 34.6%. Total porosity, effective porosity and permeability showed an increasing trend to the northwestern direction where the recharge area is located.

The concentrations of TDS and the dissolved elements are higher in the shallow groundwater compared to the deeper one, which could be related to soil salinity and evaporation processes. Ion exchange, water–rock interaction and evaporation processes are the main geochemical processes affecting the chemistry of the studied groundwater. Sodium chloride/bicarbonate types

* Corresponding author.

Peer review under responsibility of National Research Institute of Astronomy and Geophysics.

ELSEVIER Production and hosting by Elsevier

http://dx.doi.org/10.1016/j.nrjag.2015.12.001

are the most common chemical types in the study area. Most of the water samples are of old meteoric origin (Na_2SO_4 type) and old marine origin ($MgCl_2$ type). On the basis of SAR and EC values it is concluded that most of the groundwater samples are suitable for irrigation purposes.

1. Introduction

During the last 50 year, several land reclamation activities have been implemented in the West Nile Delta region. These activities were based on both surface and groundwater. This development is mainly implemented by the private sector. As the reclamation processes affect groundwater quantities and flow system, interpretation of the aquifer hydrogeological, petrophysical and hydrogeochemical characteristics can help in the understanding of the hydrogeological conditions and can also aid decision related to the quality of water intended for different uses (Hiscock, 2005).

The study area lies on the West Nile Delta, between Rosetta Branch of the River Nile and Wadi El-Natrun including Sadat City. It is bounded from south and north by the latitudes 30.0° N and 30.6° N, respectively (Fig. 1). The study area is characterized by semiarid to arid climatic conditions, where it is hot in summer, and cold to moderate in winter. It is characterized in general by a short rainy season with low and infrequent rainfall, high annual temperature variations, high evaporation and high relative humidity.

The West Nile Delta is characterized by a very gentle topography, lacking high relief and represents a part of the old alluvial plain. The surface of the area is mostly dissected by shallow drainage lines that directed either to the Nile Delta basin or to Wadi El-Natrun and Wadi El Farigh depressions. The surface geologic structure is relatively simple, although in the subsurface many complicated structures are known (Fig. 2). The West Nile Delta has a thick sedimentary succession that ranges in age from the Late Cretaceous to Quaternary.

2. Methodology

1. The evaluation of the aquifers petrophysical properties is attained through the analyses of logs of 18 selected drilled wells with depths varying from 60 m to 200 m. These wells are scattered through the study area (Fig. 3a). Well-logs interpretations were used to estimate the resistivity, total porosity, effective porosity, formation factor, permeability and shale volume.
2. Groundwater was sampled according to the standard sampling methods. Fifty-one water samples were collected from the study area representing the studied aquifers (Fig. 3b). Temperature, TDS, EC and pH were measured in situ. Water levels of the observation wells were measured by water level meter.
3. Hydrochemical analyses of the collected groundwater samples were done in the central laboratory for environmental quality monitoring in the National Water Research Center, Egypt. Titration methods are used for determining the concentration of carbonate, bicarbonate, calcium

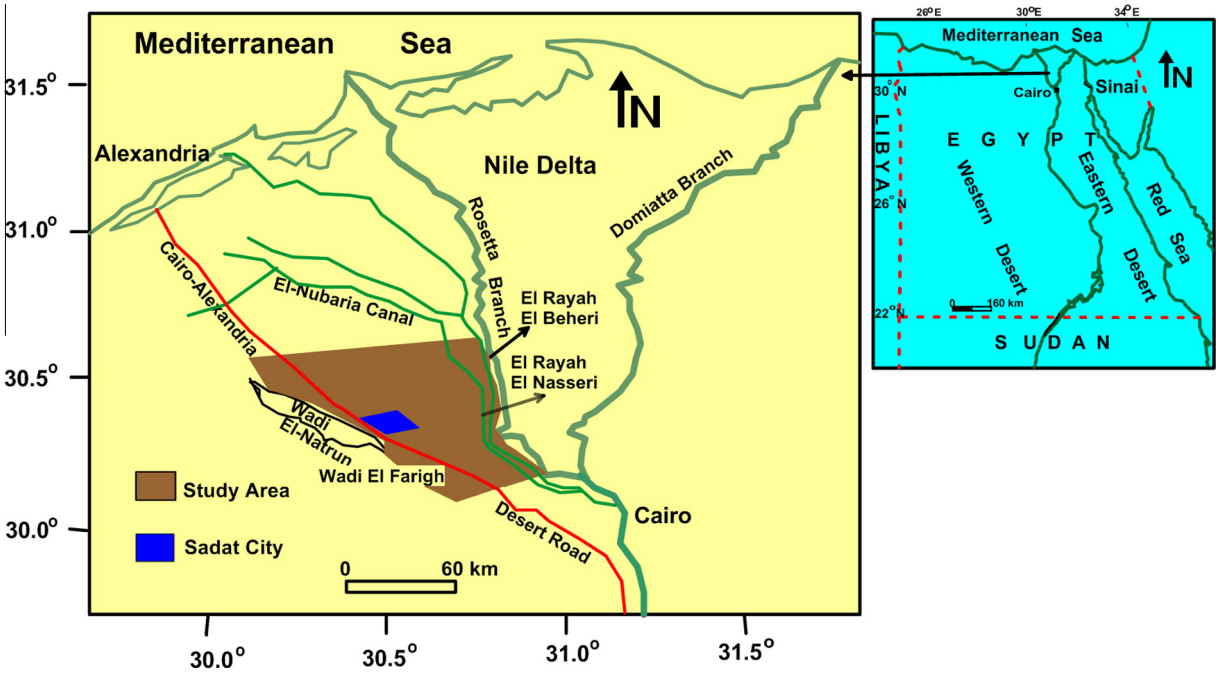

Figure 1 Location map of the study area.

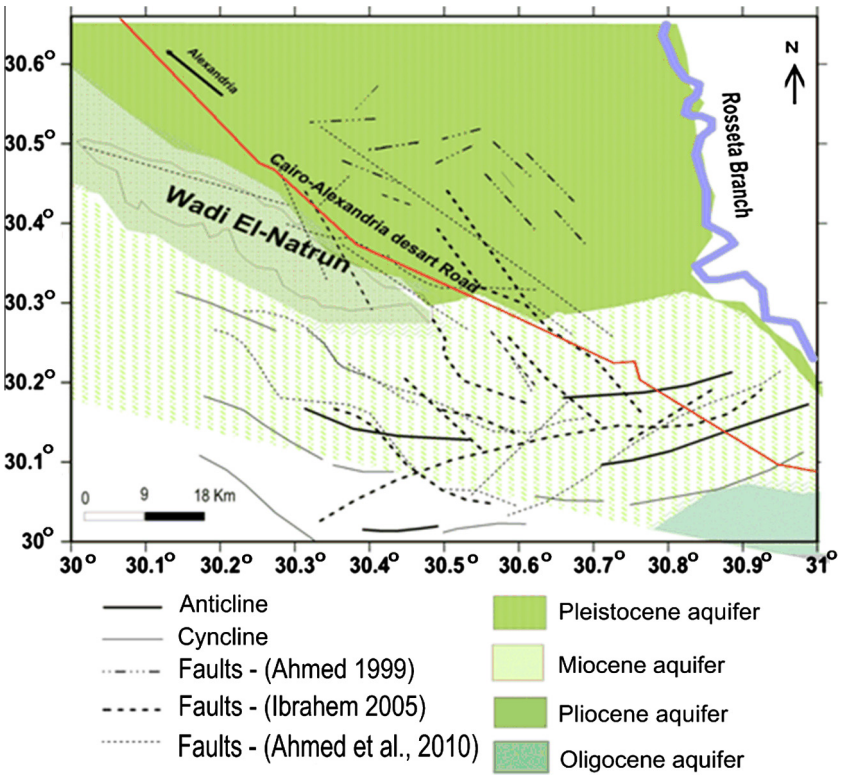

Figure 2 Hydrogeological and structural map of the study area. (See above-mentioned references for further information.)

hardness, magnesium hardness and chloride. Atomic absorption spectrometer is used for determining sodium and potassium. Spectrophotometer is used for measuring the nitrate and sulfate concentrations. The measured hydrochemical parameters are listed in Table 1.

3. Aquifer systems

The water-bearing formations in the investigated area are classified into four aquifers: The Quaternary, Pliocene, Miocene and Oligocene aquifers (Fig. 2). These aquifers are hydraulically connected and considered as one hydrological unit. The Quaternary aquifer occupies the major part of the investigated area and it is essentially composed of fluviatile graded sand and gravel intercalated with thin clay lenses (El-Gamal, 2005). The Quaternary aquifer is mainly recharged from the Nile water, infiltration of irrigation water and from the adjacent canals. The discharge from this aquifer can happen naturally or artificially. Natural discharge occurs mainly through other aquifers. The artificial discharge occurs through hundreds of productive wells.

The Pliocene aquifer is mainly restricted to Wadi El-Natrun depression; its sediments are composed of clay facies with interbeds of water bearing sandy layers. The thickness of the aquifer deposits is about 140 m at Wadi El-Natrun, with a saturated thickness of about 90 m. The Miocene sediments are represented by the Moghra Formation, and are mainly composed of sand, sandstone and clay interbeds with vertebrate remains and silicified wood (Said, 1962). These sediments are occasionally overlain by the Quaternary deposits and are underlain by the Oligocene basaltic sheet. The total thickness of the Miocene sediments reaches about 250 m at Wadi El-Natrun, and regionally this thickness increases in northwest direction (El Ghazawi and Atwa, 1994).

Oligocene aquifer consists of sands and gravels with clay interbeds as well as thin limestone bands at the base and thick (30 m) basaltic sheet at top. The Oligocene sediments fill the main channel of Wadi El-Natrun with a total thickness of about 400 m. The Oligocene aquifer is located west of Cairo. Abdel Baki (1983) mentioned that it is recharged from rainwater of recent and past periods.

The constructed piezometric map (Fig. 4) reveals the following: (a) the groundwater movement takes a direction from the east and north where the surface water sources are located to the west and south directions; (b) Wadi El-Natrun acts as natural discharge areas for the groundwater; and (c) the hydraulic gradient increases gradually from east to west with a marked increase close to Wadi El-Natrun that is related to natural discharging effect and to the presence of fault lines (Fig. 2) around both the eastern and northern sides of Wadi El-Natrun depression (Abdel Baki, 1983).

A difference map (Fig. 5) was constructed to show the water table change between 1960 and 2010. Drawdown of the groundwater levels has been occurred mainly in the southern part of the region, near the Cairo–Alexandria desert road, which could be related to extensive groundwater exploitation in the central and southern parts of the study area. The drawdown reached about 25 m at south Khatatba and Wadi El-Farigh. On the long term, this can lead to aquifer depletion, while in the short and medium term a large part of the existing wells will fall dry. The drilling of new wells with greater depths will affect the economic viability of the development projects. On the other hand, Infiltration from irrigation channel and

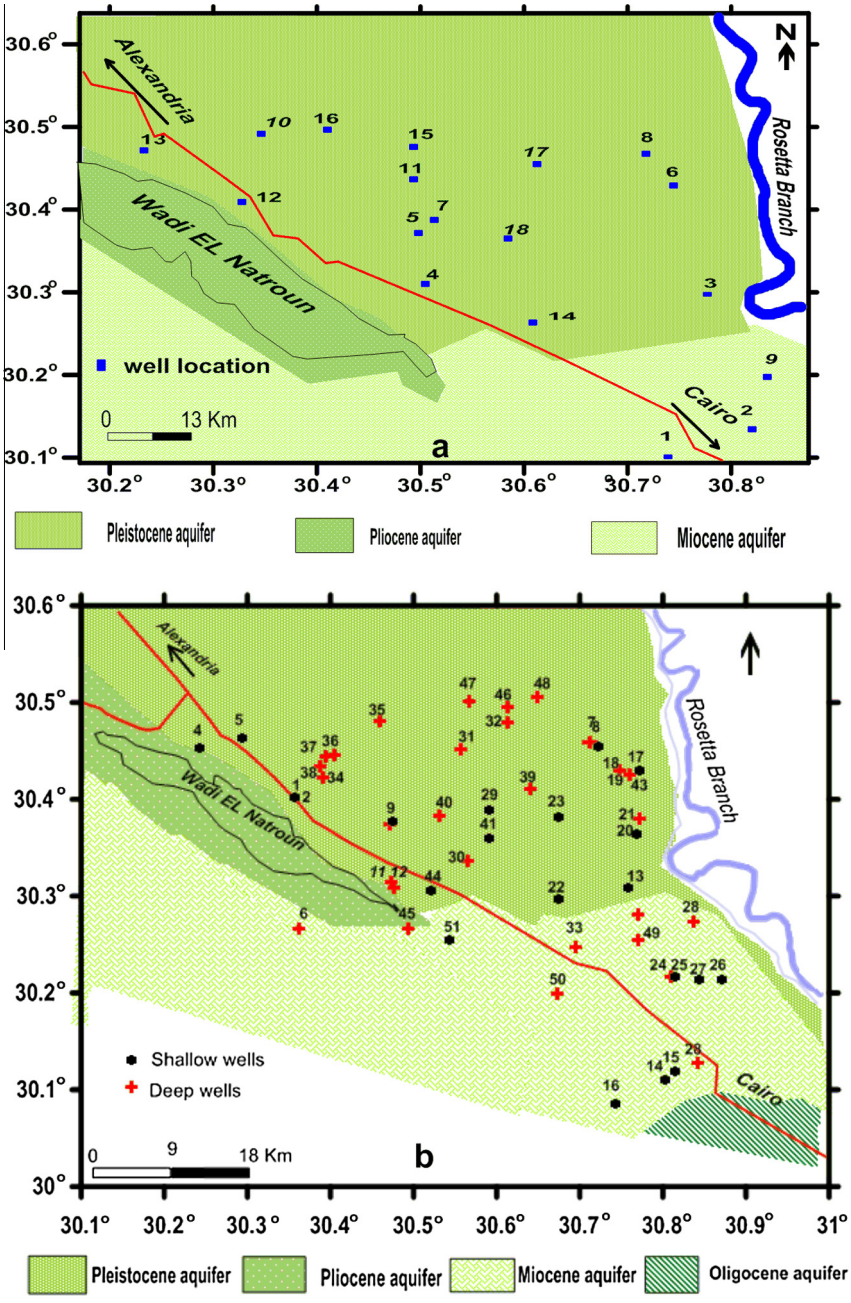

Figure 3 Location map of the selected wells for log analysis (a) and well location map of the collected groundwater samples (b).

excess uses of surface water for irrigation at the northern part of the area led to water level rise about 5 m to the east and 10 m to the west.

4. Petrophysical characteristics

4.1. Electric logs

The electric log is an excellent correlation tool; this means that the electric log gives a good indication on the general type of material of which each bed is composed. Also it is possible to determine the amount of pore space contained in the formation and the amount and kind of fluids contained in the pore space.

The formation water resistivity (R_w) for the Quaternary and Miocene aquifers is computed using Archie (1942) equation:

$$R_w = (R_{mf} * R_t)/LLS$$

R_{mf} is the resistivity of the mud filtrate which is depending on the temperature of the mud.

R_t is the true resistivity which can be computed from long normal resistivity (LLD) and short normal resistivity (LLS) by using a formula.

Table 1 Chemical compositions of the collected groundwater samples.

S. no.	TDS (ppm)	Ec	pH	Ca	Na	Mg	K	HCO_3	Cl	SO_4	NO_3
				(ppm)							
1	346	542.0	8.11	22.4	51.0	14.0	8.1	143.9	62.0	41.2	1.1
2	662	1035.0	7.56	19.8	200.0	7.3	9.4	162.6	238.2	52.6	3.4
3	531	830.0	7.93	34.4	96.0	26.0	7.3	259.1	113.4	34.5	2.3
4	3123	4880.0	7.74	132.8	794.0	80.0	12.7	214.9	1220.0	426.3	4.8
5	2502	3910.0	7.67	122.0	596.0	66.5	20.4	302.1	755.3	755.3	16.2
6	921	1439.0	7.91	70.0	215.0	24.0	9.6	266.0	300.0	100.0	0.3
7	1958	3060.0	7.96	150.0	490.0	38.7	18.0	200.0	750.0	350.0	6.5
8	225	352.0	7.37	28.0	20.0	15.1	6.0	150	26.0	24.0	1.0
9	753	1177.0	8.72	50.9	180.0	15.4	7.0	164.6	230.0	120.0	0.0
10	839	1311.0	8.15	59.2	210.0	12.7	8.0	153	310.0	110.0	0.0
11	885	1383.0	8.69	62.0	200.0	14.5	8.0	175.8	280.0	120.0	0.0
12	729	1139.0	7.84	53.8	180.0	15.6	6.0	170	240.0	115.0	7.6
13	1898	2970.0	7.5	142.0	440.0	40.2	12.0	310	650.0	300.0	30.0
14	528	824.0	7.69	54.3	100.0	14.5	6.0	185	150.0	50.0	0.7
15	456	712.0	7.79	49.8	80.0	13.2	6.0	217	110.0	22.0	0.2
16	753	1177.0	7.78	54.1	180.0	14.4	6.0	227	210.0	112.0	0.7
17	1632	2550.0	7.93	14.0	215.0	251.3	52.2	204	329.0	556.0	120.0
18	421.9	754.0	7.04	97.1	139.0	37.0	100.0	183	55.0	139.0	0.0
19	349	545.0	7.28	7.0	30.0	53.3	17.0	180	40.0	70.0	1.4
20	878	1372.0	7.22	9.0	145.0	100.0	25.0	200	200.0	219.0	0.0
21	1954	3060.0	7.07	12.0	290.0	238.0	70.0	350	440.0	570.0	0.0
22	1902	2970.0	7.29	10.0	285.0	224.0	72.5	342	410.0	550.0	54.7
23	1902	2970.0	7.31	11.0	278.0	234.0	71.5	350	415.0	545.0	49.0
24	1280	2010.0	7.45	21.0	263.0	130.6	32.5	310	340.8	281.6	15.4
25	693	1080.0	7.58	15.0	134.0	59.1	17.5	240	174.4	79.1	0.6
26	2726	4260.0	7.36	28.0	480.0	361.4	35.6	341.1	707.6	784.0	30.4
27	921	1440.0	7.4	12.0	206.0	77.4	17.7	226.4	290.2	112.3	6.2
28	748	1440.0	7.49	11.0	96.0	112.0	22.4	220.1	130.1	216.0	0.7
29	758	1010.0	8.1	43.0	166.0	18.0	6.0	275	128.0	123.0	2.5
30	567	800.0	7.91	32.0	138.0	13.0	7.0	171	178.0	171.0	4.0
31	628	910.0	8.01	36.0	152.0	9.0	4.0	158	112.0	158.0	3.0
32	791	1100.0	8.01	57.0	157.0	19.0	4.0	298	146.0	110.0	4.0
33	431	1760.0	7.41	28.0	66.0	22.0	7.0	195	89.0	24.0	1.3
34	600	900.0	7.5	45.0	40.0	11.0	3.0	180	140.0	160.0	0.0
35	679	720.0	7.6	60.9	238.1	23.6	5.3	494	290.5	203.5	2.2
36	306.6	1050.0	7.7	10.8	130.9	11.2	6.6	219.6	35.5	126.8	1.1
37	329.6	1100.0	7.7	37.2	42.1	15.7	4.8	201.3	35.5	18.8	1.2
38	352	1200.0	7.7	19.4	45.1	15.8	4.7	231.8	17.8	27.3	2.1
39	229.8	2230.0	8.3	36.1	27.8	9.8	5.0	185.7	28.4	5.7	0.8
40	321.9	2060.0	7.7	28.1	57.9	9.8	5.0	134.9	42.5	57.5	0.1
41	307.2	4100.0	7.5	24.0	40.7	12.2	5.0	151	40.5	39.4	0.3
42	487	660.0	8.06	42.0	77.0	14.0	7.0	256	70.0	19.0	6.0
43	550	830.0	8.14	24.0	117.0	28.0	8.0	153	178.0	43.0	7.0
44	1728	1690.0	7.3	148.3	308.0	70.8	11.0	140.8	584.9	283.7	0.9
45	343	960.0	7.8	16.0	128.3	7.3	3.0	176	56.7	103.0	0.5
46	315	2080.0	8	32.1	36.7	14.6	5.0	159.1	28.4	33.9	0.3
47	482.6	3200.0	8.3	48.1	97.2	31.7	7.0	174	117.0	125.9	8.3
48	220	2000.0	8.3	28.1	24.3	12.2	5.0	165	28.4	10.0	0.4
49	648	950.0	8.1	38.0	156.0	12.0	8.0	191	138.0	106.0	3.0
50	799	1170.0	8.2	35.0	196.0	16.0	9.0	246.0	161.0	136.0	4.0
51	515	430.0	8.1	46.0	138.0	15.0	3.0	183.0	42.0	89.0	2.0
Average	880.5	1.6	7.8	44.5	179.9	53.0	16.0	219.3	232.6	177.0	8.0

if LLD > LLS R_t = 1.7LLD-0.7LLS
if LLD < LLS R_t = 2.4LLD-I.4LLS
(Schlumberger log interpretation principles, 1972)

The computations show that, the maximum R_w of the water zone in the Quaternary aquifer attains 20.3 ohm m at well (14) and the minimum R_w reached 9.6 ohm m at well (3), while the maximum R_w of the water zone in the Miocene aquifer attains 15.96 ohm m at well (1) and the minimum R_w reached 10.6 ohm m at well (2). Generally, the areal distribution of the estimated formation water resistivity in the Quaternary

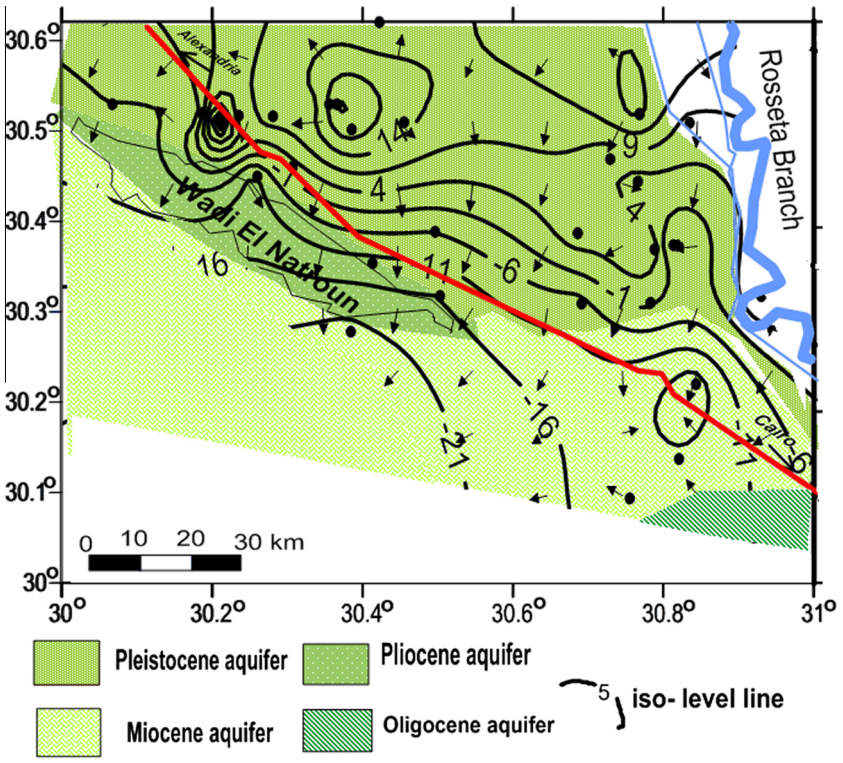

Figure 4 The water table and groundwater flow direction (current study, 2010).

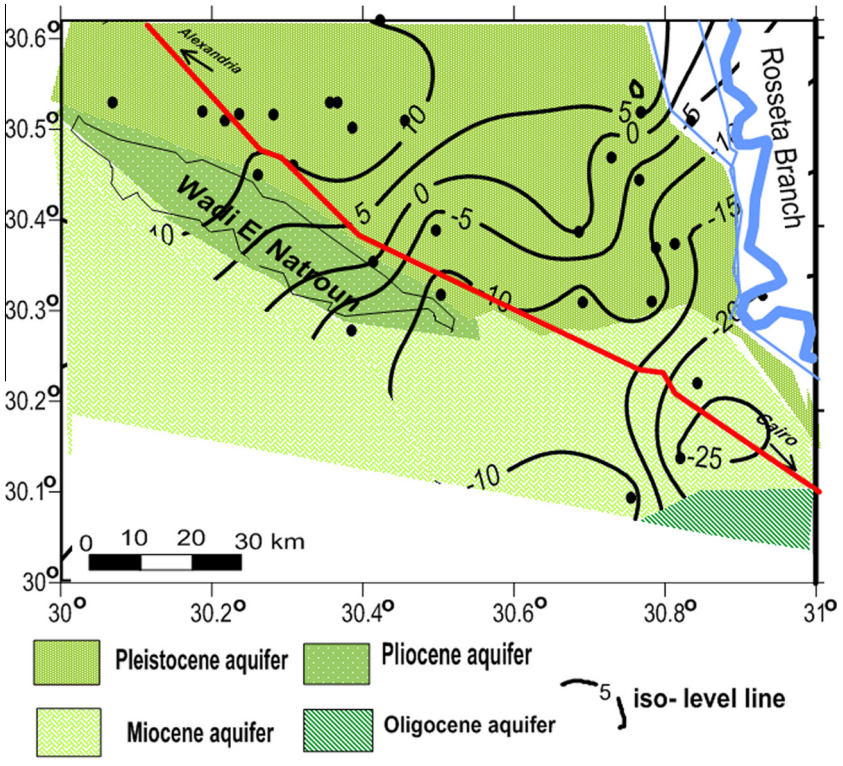

Figure 5 Difference map shows the drawdown in the groundwater levels (negative values) and water level rise (positive values) between 1960 and 2010.

aquifer is increased to the central part as indicated in Fig. 6a and increases in Miocene aquifer to the west.

The Formation Factor is the ratio of the resistivity of a formation to the resistivity of water with which it is saturated, while formation factor is, strictly speaking, defined only for clean brine-saturated sands (for which it is nearly independent of the fluid resistivity). Because most of the rock grains have a very high resistance relative to water, the formation factor is roughly greater than (1). The smaller the grain size, the smaller the value of formation factor. The formation water resistivity factor (F) increases as the grain size increases and decreases as water formation resistivity (R_w) increases. The average values of the formation factor (F) for The Quaternary aquifer show that the maximum value attains 5.28% at well (10), while the minimum value reaches 2.28% at well (13). Generally, the formation factor (F) of the Quaternary aquifer is increased toward the northwest direction as shown in Fig. 6b. The formation factor (F) for The Miocene aquifer shows that the maximum value attains 16.58% at well (2), while the minimum value reaches 6.55% at well (1). Generally, the formation factor (F) of the Miocene is increased toward the southeast direction as shown in Fig. 6b.

The formation resistivity factor is a function of porosity, and also of pore structure and pore size distribution. The formula relating porosity and formation factor, is shown as follows:

$$F = 0.62/(\Phi)^{2.15} \quad \text{for sand}$$

and

$$F = 1/(\Phi)^{2} \quad \text{for formation factor}$$

The first relationship is popularly referred to as the Humble formula and the second, as the Archie formation factor relationship.

$$\text{Then} \quad R_t/R_w = 0.62/(\Phi)^{2.15} \quad \text{for sand (Humble formula)}$$

By applying the above equation (Humble formula) into the Quaternary and Miocene aquifers, after obtaining F, R_t and R_w, the average porosity (Φ %) of water zones could be obviously obtained.

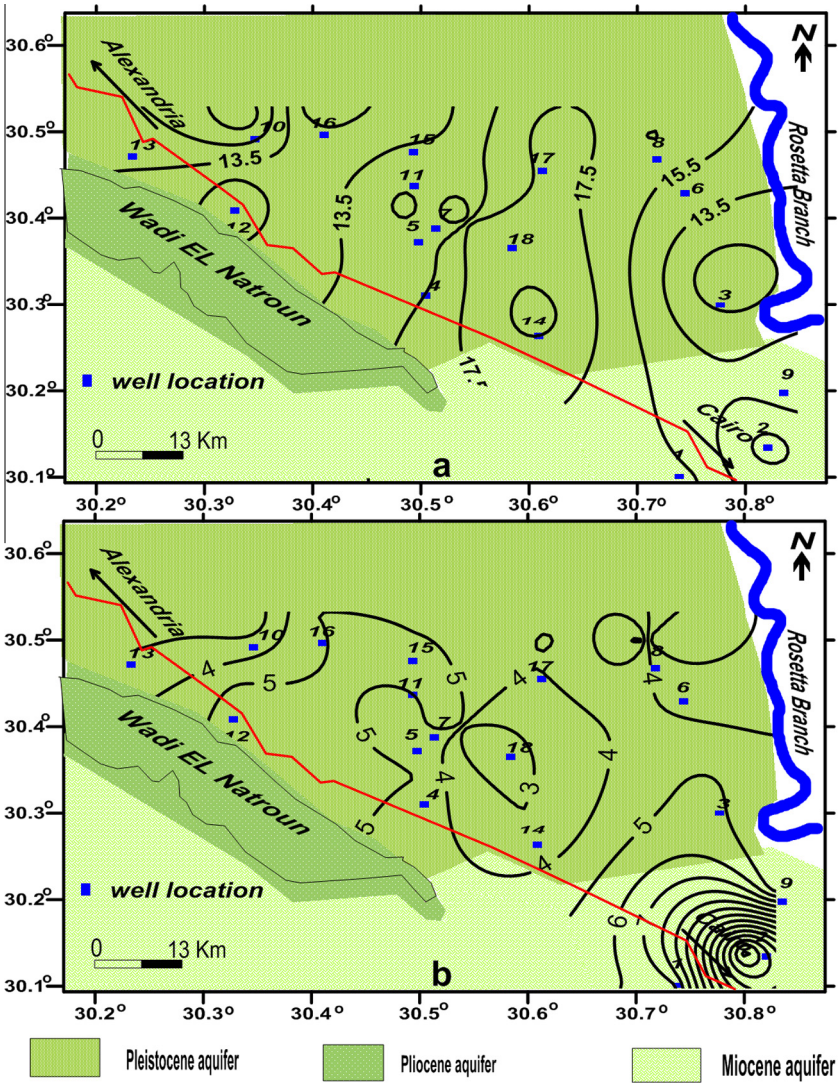

Figure 6 Spatial distribution of formation water resistivity (a) and formation resistivity factor (b).

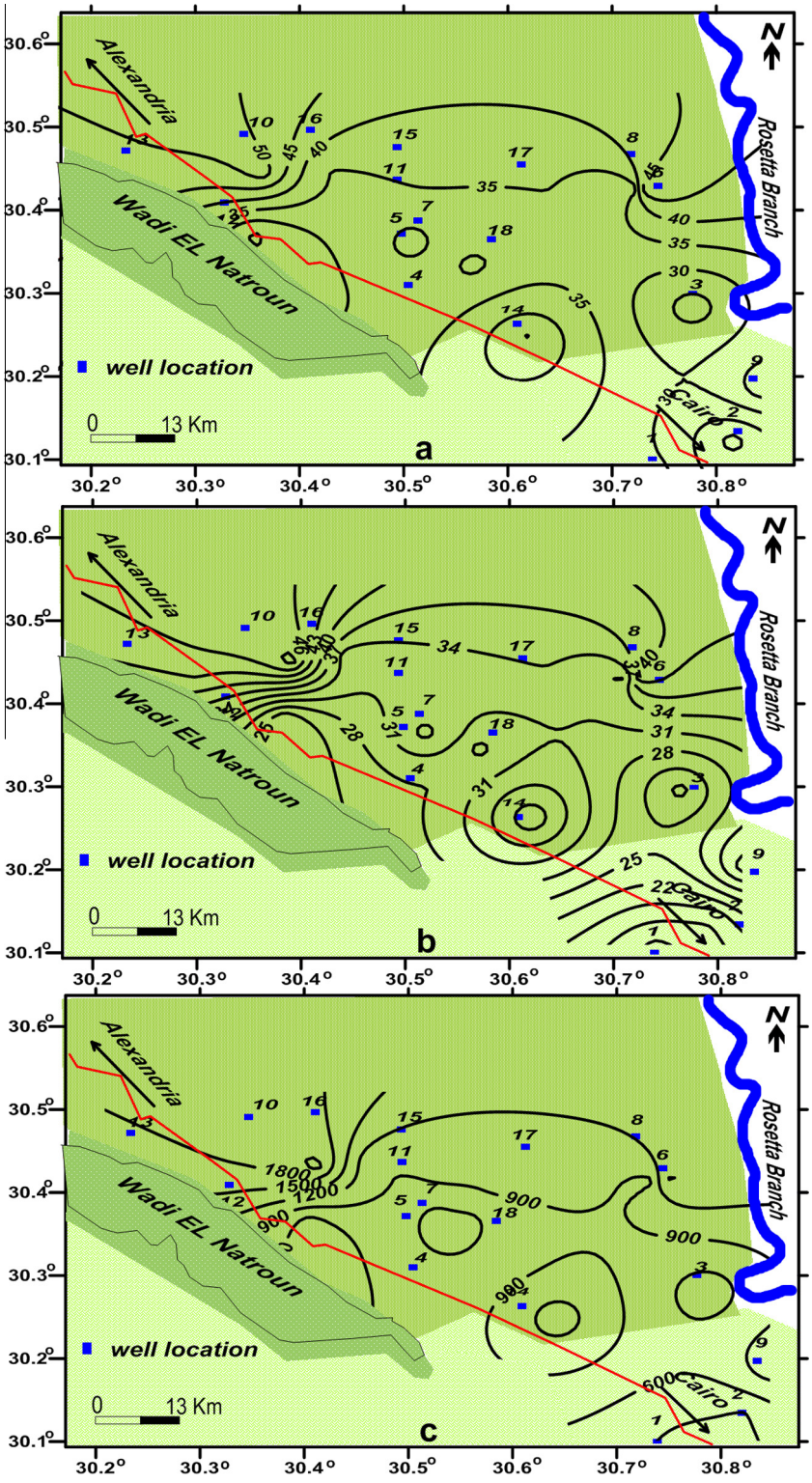

Figure 7 Spatial distribution of (a) total porosity, (b) effective porosity, (c) permeability and (d) volume share of shale.

Formation Effective Porosity is the share of the pore space through which the groundwater flows under normal pressure condition. Generally, Effective Formation Porosity (Φ_{eff} %) is a function with Formation water (F %) and a function with the TDS of water flows through pore space under normal pressure condition.

Then

$\Phi_{eff} = (R_w * 10{,}000/R_t)^{1/2}$	for Sodium Carbonate
$\Phi_{eff} = (R_w * 3500/R_t)^{1/2}$	for Sodium Chloride (Guyod, 1966)

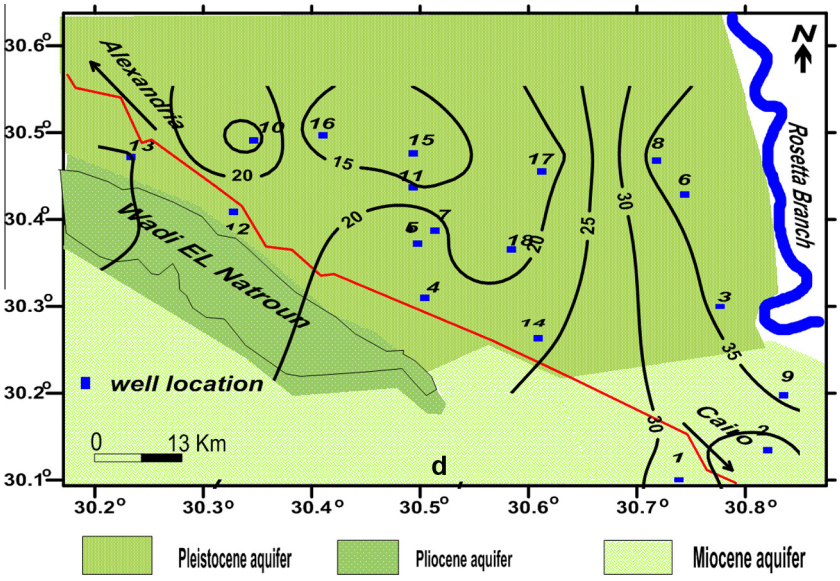

Fig. 7 (*continued*)

where Φ_{eff} is the effective porosity, R_w is the formation water resistivity, and R_t is the true resistivity which is obtained from long normal resistivity (LLD).

The obtained average total porosity and effective porosity for the Quaternary and the Miocene aquifer are shown in Fig. 7a and b. The maximum average total and effective porosity (Φ %) in the Quaternary, attains 52.1% and 47% respectively, at well (10) while the minimum average total and effective porosity attains 25.2% and 24.8% respectively, at well (1). The porosity increases toward the northern and northwestern directions where the recharge area is located. In the Miocene aquifer the maximum average total and effective porosities are 36.3% and 35.4% respectively, at well (9) while the minimum average is 18.3% and 15.3% respectively, at well (2) and well (1). The porosity and effective porosity increases toward the north direction (Fig. 7a and b). Generally, the average porosity and the average effective porosity of the two aquifer increase as the thickness, and sand percentage increase toward north direction.

Some rough relationships between effective porosity and permeability are existed, and greater permeability in general corresponds to greater effective porosity, but this is far from being an absolute rule. Shale and some sand have high porosity, but the grains are so small that the path available for the movement of fluid is quite restricted and tortuous; thus, their permeability may be very low. Recently, Jorgensen (1988 and 1989) reported on permeability estimating procedures that require data only on the cementation exponent (n) and effective porosity (Φ_{eff}). Jorgensen equation for estimating permeability (K) in millidarcies is as follows:

$$K = 84,000\left(\Phi_{eff}^{n+2}\right)\Big/\left(1-\Phi_{eff}\right)^2$$

where

K is the permeability in millidarcy.
Φ_{eff} is the effective porosity (%).
n is the cementation factor or exponent that equal 2.15 for sand.

By applying the above equation, the estimated permeability of the Quaternary aquifer increases toward the northwest directions, as illustrated in (Fig. 7c) and that of Miocene aquifer decreases toward the south direction. The higher permeability of the Quaternary aquifer compared to Miocene aquifer is due to the higher percentage of shales in the latter aquifer. The higher permeability in the northwestern direction is the cause for being a good recharge area as mentioned in the hydrogeology section.

4.2. Gamma logs

The gamma logs are used for determining the shale content. This estimation follows a linear relation which is applied as follows:

$$V_{sh} = (G_{log} - G_{min})/(G_{max} - G_{min}) \quad \text{(Schlumberger, 1972)}$$

where

V_{sh} is the shale content or volume share of shale.
$G_{\log}$ is the gamma activity of the material (formation) at certain depth.
$G_{\min}$ is the gamma activity of clean sand.
$G_{\max}$ is the gamma activity of shale in the formation.

The determination of the average volume share of shale in the Quaternary formation shows that the maximum volume share of shale attains 38.3% at well (8) while the minimum volume attains 12.1% at wells (16). The volume share of shale increased to the east and southeast directions. In the Miocene Formation, the maximum volume share of shale attains 37.6% at well (9) while the minimum value attains 27% at well (2). The volume share of shale increased to the east directions (Fig. 7d).

Generally, the volume share of shale increases toward the east and the south directions. As mentioned before, where V_{sh} increases the permeability decreases. The recharge area located to the northwestern direction has higher values of porosity, effective porosity and permeability. On the other

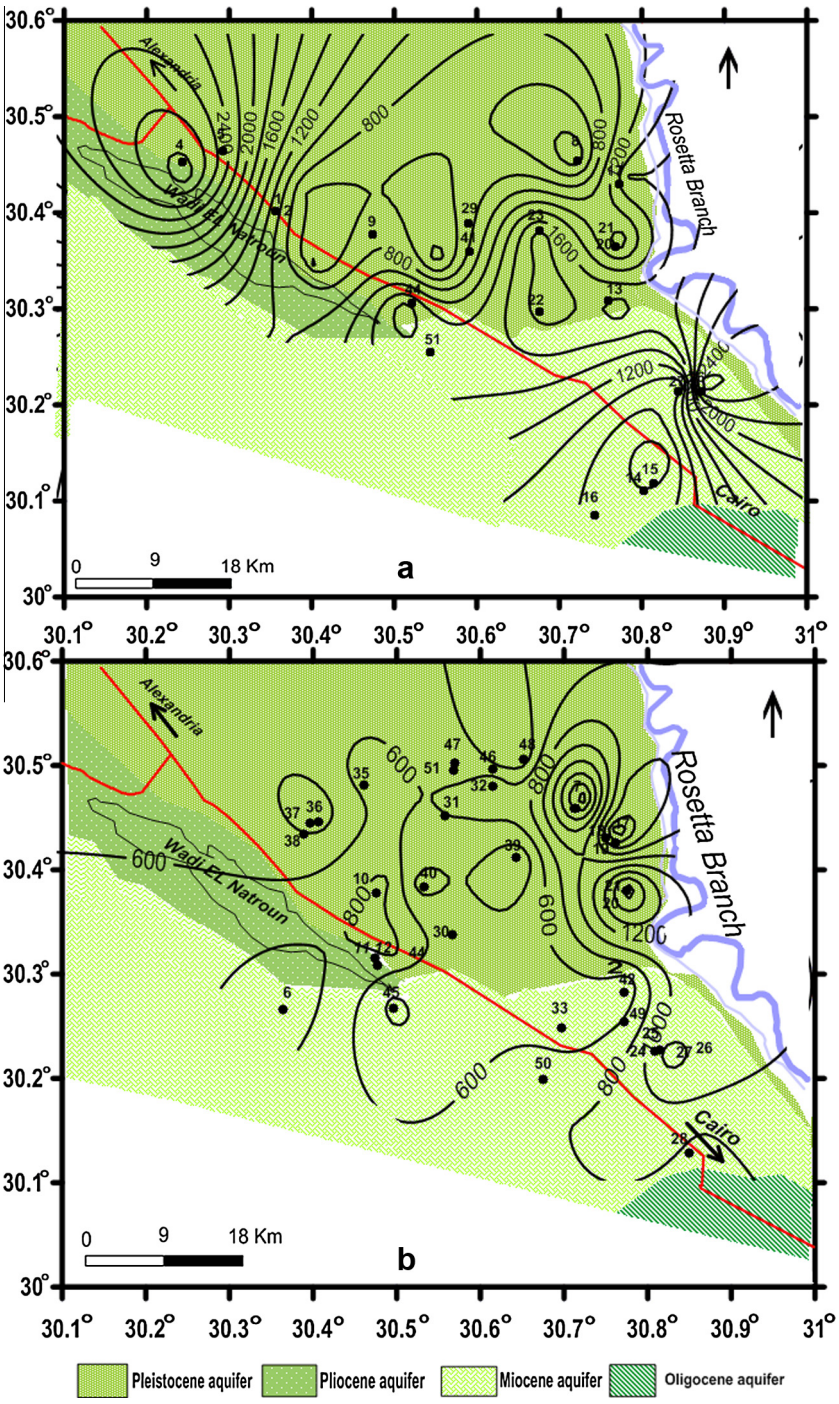

Figure 8 Water salinity distribution map in the shallow zones (a) and deep zones (b).

hand, the recharge area has lower values of volume share of shale. This phenomenon helps in increasing the infiltration from the irrigation channels.

5. Hydrogeochemistry

5.1. Hydrochemical characteristics

The collected samples have pH ranges from 6.6 to 8.8 with an average 7.8. The specific conductance of the groundwater samples ranged between 285 and 4390 mS/cm with an average 1650 mS/cm (Table 1). Contour maps for the shallow and the deep groundwater zones are prepared in the present study to illustrate the vertical and lateral change in the chemical properties and major ions concentrations. Wells less than 80 mbsl (meter below sea level) deep were considered shallow and those deeper than 80 mbsl were considered deep.

According to Winslow and Kister (1956), the salinity values of the studied groundwater samples vary in the range from 225 to 3123 mg/l. The majority of the samples fall in the fresh water

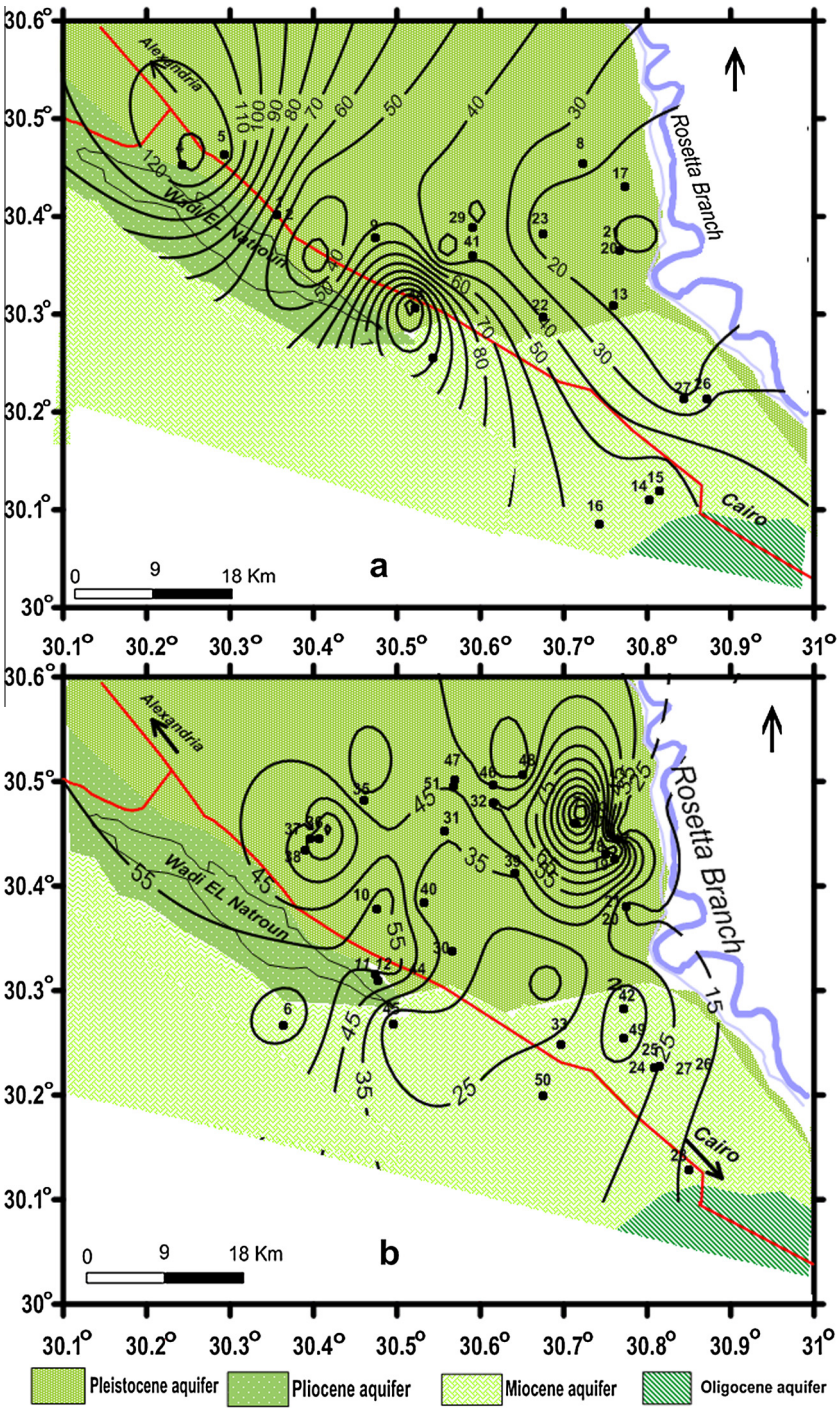

Figure 9 Iso-calcium contour maps of shallow groundwater (a) and the deep groundwater (b).

categories; about 73.4% of the samples have TDS varying in the range from 225 mg/l to less than 1000 mg/l, about 24.4% of the samples have TDS range from 1000 to 3000 mg/l and only 2.2% of the samples have TDS more than 3000 mg/l. Distribution of water salinity in the shallow zones of the Pleistocene aquifer shows a gradual increase toward the east and northwest directions (Fig 8a). The high salinity in the mentioned directions is probably attributed to the effect of intensive use of water for irrigation water, while soils have higher salinity. Evaporation might play an important role especially in the northwestern part of the area. In deep zones, there is a gradual increase in the water salinity toward the northwest direction due to water rock interaction (Fig. 8b). Generally, the shallow groundwater of the Pleistocene aquifer has higher TDS than the deeper one because the former is affected by soil and surface evaporation processes while the deeper is directly recharged from the Nile water. In shallow zones of the Miocene aquifer, there is a gradual increase in the water salinity toward the eastern direction, while, in deep zones there is a gradual decrease in the water salinity toward the northwest direction.

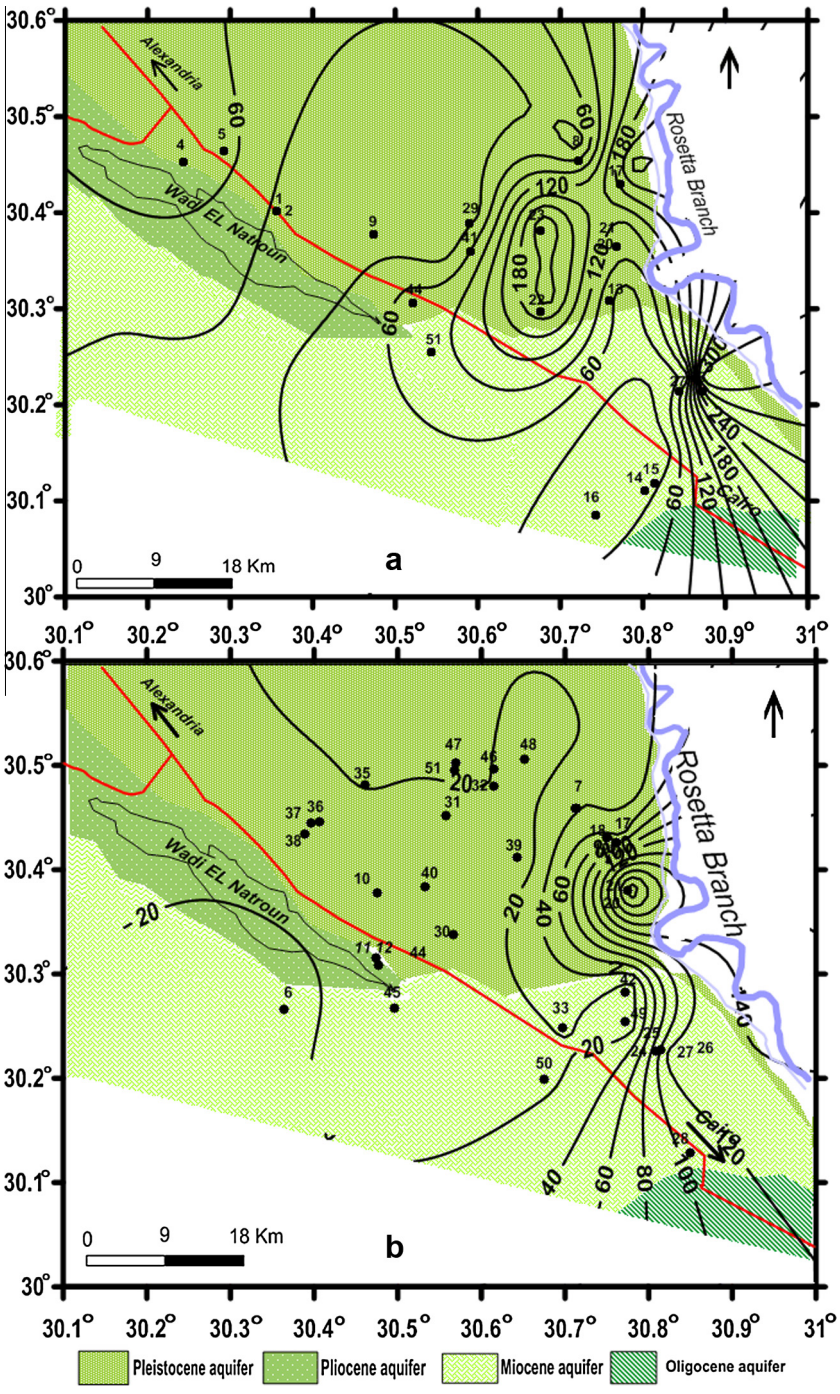

Figure 10 Iso-magnesium contour maps of the shallow groundwater (a) and the deep groundwater (b).

Calcium content ranges between 7 and 148 mg/l with an average 44 mg/l (Table 1). Distribution of calcium in the shallow zones of the Pleistocene aquifer (Fig. 9a), indicates that there is a gradual decreasing trend of calcium content to the eastern and southern part which is due to the seepage of freshwater from the River Nile and irrigation system. In deeper zone (Fig. 9b) calcium reaches its minimum concentration in the central part with increasing trend to the east and the west.

Distribution of calcium in the Miocene aquifer (Fig. 9a and b), indicates that there is a gradual decrease of calcium content to the eastern and southern directions for the deeper and shallower groundwater, respectively. This might be due to the seepage of freshwater from the irrigation system. The concentration of calcium increases westwards probably due to the dissolution of calcium containing minerals of the aquifer sediments. Generally, calcium content in the shallow zones is higher than that of the deep zones.

The concentration of magnesium ion in the collected samples ranges between 7 and 361 mg/l with an average 53 mg/l. Fig. 10a, shows the regional increase of magnesium ion concentration to the central and eastern parts of the area in the

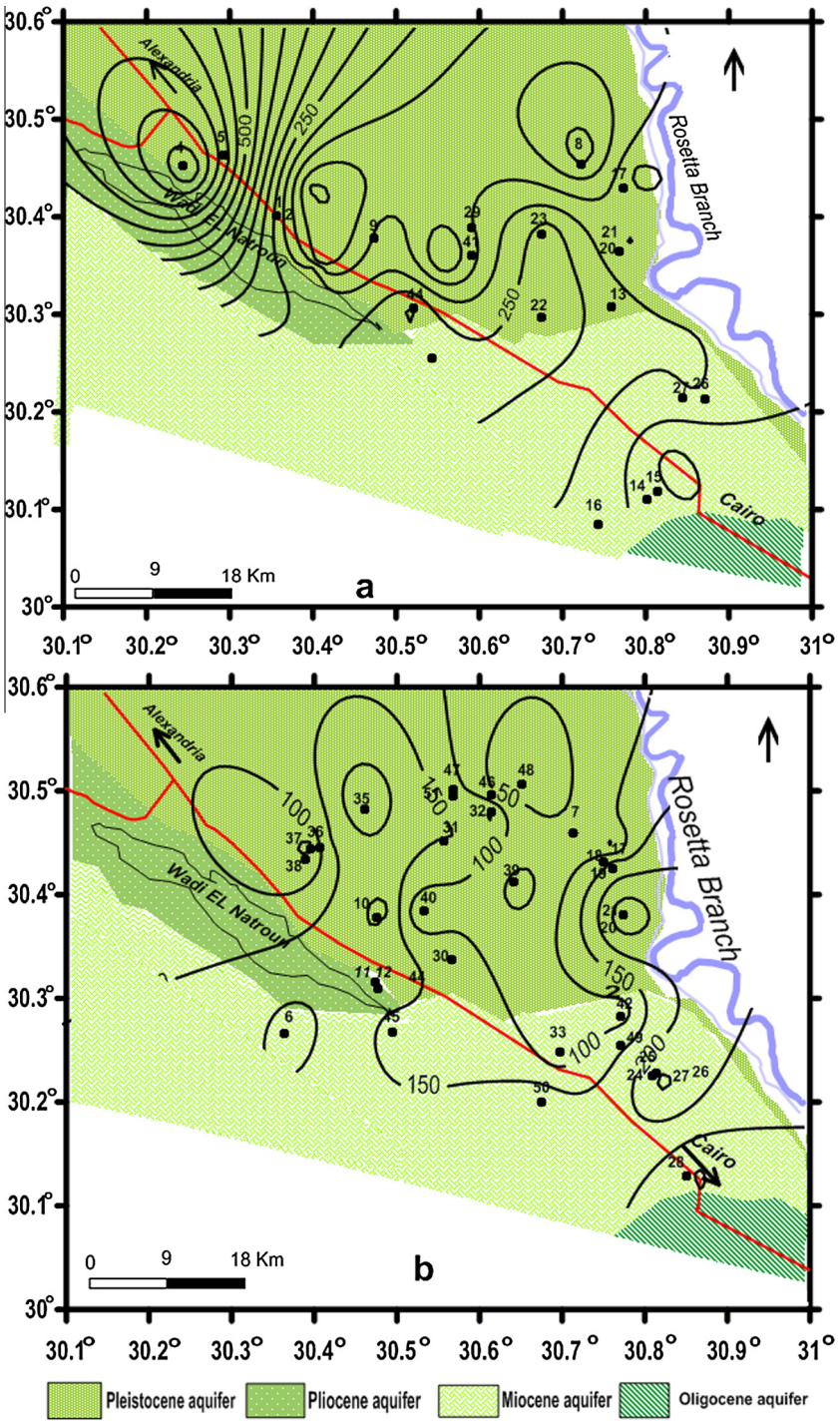

Figure 11 Iso-sodium contour maps of the shallow groundwater (a) and the deep groundwater (b).

shallow zones of the Pleistocene aquifer, while in the deeper zones of the same aquifer, magnesium concentration does not vary greatly in the western part and increases to the east (Fig. 10b). In the Miocene aquifer, magnesium concentrations increase to the east in the shallow and deep zones.

The sodium ion concentration ranges between 20 and 794 mg/l with an average 180 mg/l (Table 1). In the shallow zones of the Quaternary aquifer, the groundwater of the eastern area near Rosetta Branch has the lowest sodium content (Fig. 11a), while that in the northwest has the highest Na content. According to the groundwater flow system (Fig. 4), this distribution pattern is related to recharge source and effect of evaporation processes. The deeper groundwater of the same aquifer has lower Na content compared to that of the shallow groundwater (Fig. 11b). This vertical change might be related to soil salinity effect on the shallow groundwater.

Generally Na content of the deeper groundwater decreases toward the central part of the area. Fig. 11a and b, shows the

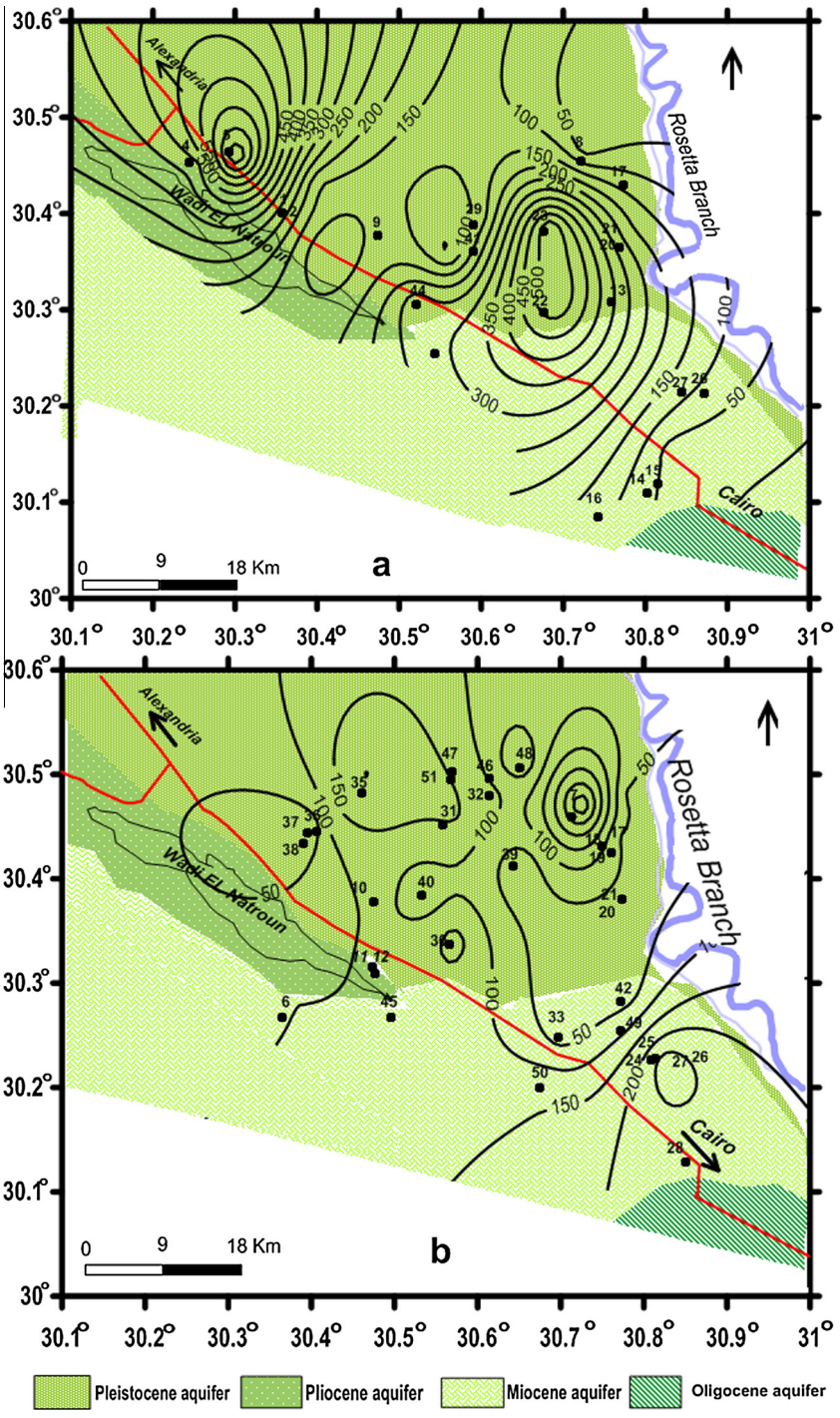

Figure 12 Iso-sulfate contour maps of the shallow groundwater (a) and the deep groundwater (b).

regional increase of sodium ion concentration in the Miocene aquifer to the west direction. In general, Na content of the Miocene aquifer is lower than that of the Quaternary aquifer.

The sulfate ion concentration varies between 6 and 784 mg/l with an average 177 mg/l (Table 1). In the shallow zones, low content of sulfate ion is observed in the eastern parts (Fig. 12a) due to seepage of freshwater through irrigation water from Rosetta Branch. Higher concentrations are observed in the central and the northwestern parts of the area. Like most of the elements, the deeper groundwater has lower content of SO_4 compared to shallow zones (Fig. 12b). Sulfate does not vary greatly in the deep groundwater of the Pleistocene aquifer but with local enrichment in the north eastern part. In the Miocene aquifer, Sulfate concentration increases southward in the deeper zones but decreases in the same direction in shallow zones.

The chloride ion concentration ranges between 17.8 and 1220 mg/l with an average 232.6 mg/l (Table 1). In the Pleistocene aquifer, the iso-concentration chloride map of the shallow groundwater (Fig. 13a) indicates a noticeable increase in

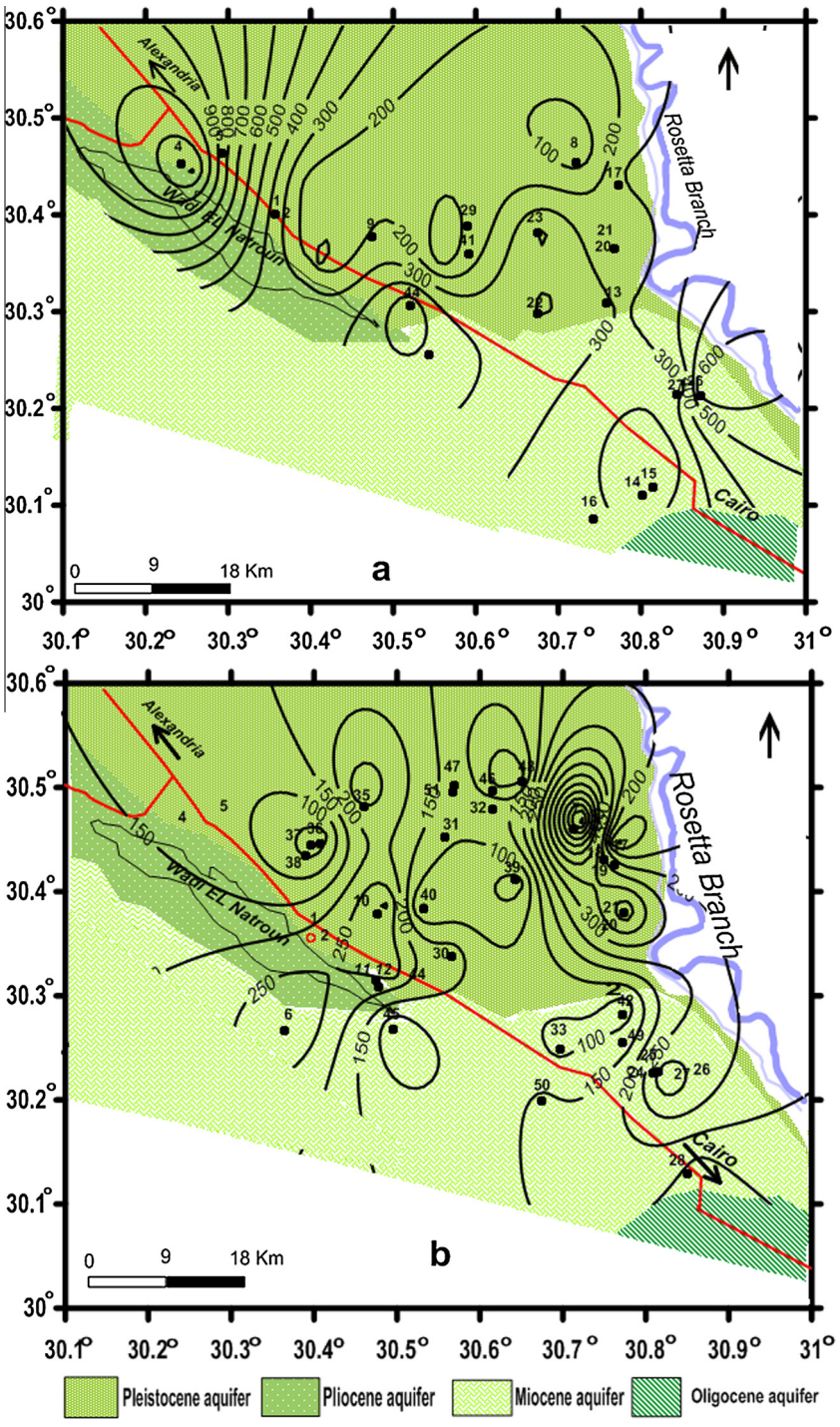

Figure 13 Iso-chloride contour maps of the shallow groundwater (a) and the deep groundwater (b).

the chloride ion concentrations toward the northwest, and decrease toward Rosetta branch to the east. This difference might be related to soil salinity and evaporation effects. In the deep zones (Fig. 13b), chloride concentration is lower than that of the shallow zones and the highest values are located to the east. In the Miocene aquifer (Fig. 13) it is observed that the chlorite ion concentration increased to south and east.

The bicarbonate ion concentration ranges from 135 to 494 mg/l with an average 219 mg/l (Table 1). In general, the iso-bicarbonate distribution map (Fig. 14a and b) in the Quaternary aquifer shows an increasing toward the central part in the shallow zones and to the north in the deep zones. Such distribution could be related to the CO_2 effect on the infiltrated shallow groundwater on the eastern part of the area. But in the deeper zones, higher bicarbonate content in the northern part could mainly be related to carbonate mineral dissolution or chemical weathering. In the Miocene aquifer (Fig. 14a and b) bicarbonate has a little change in both

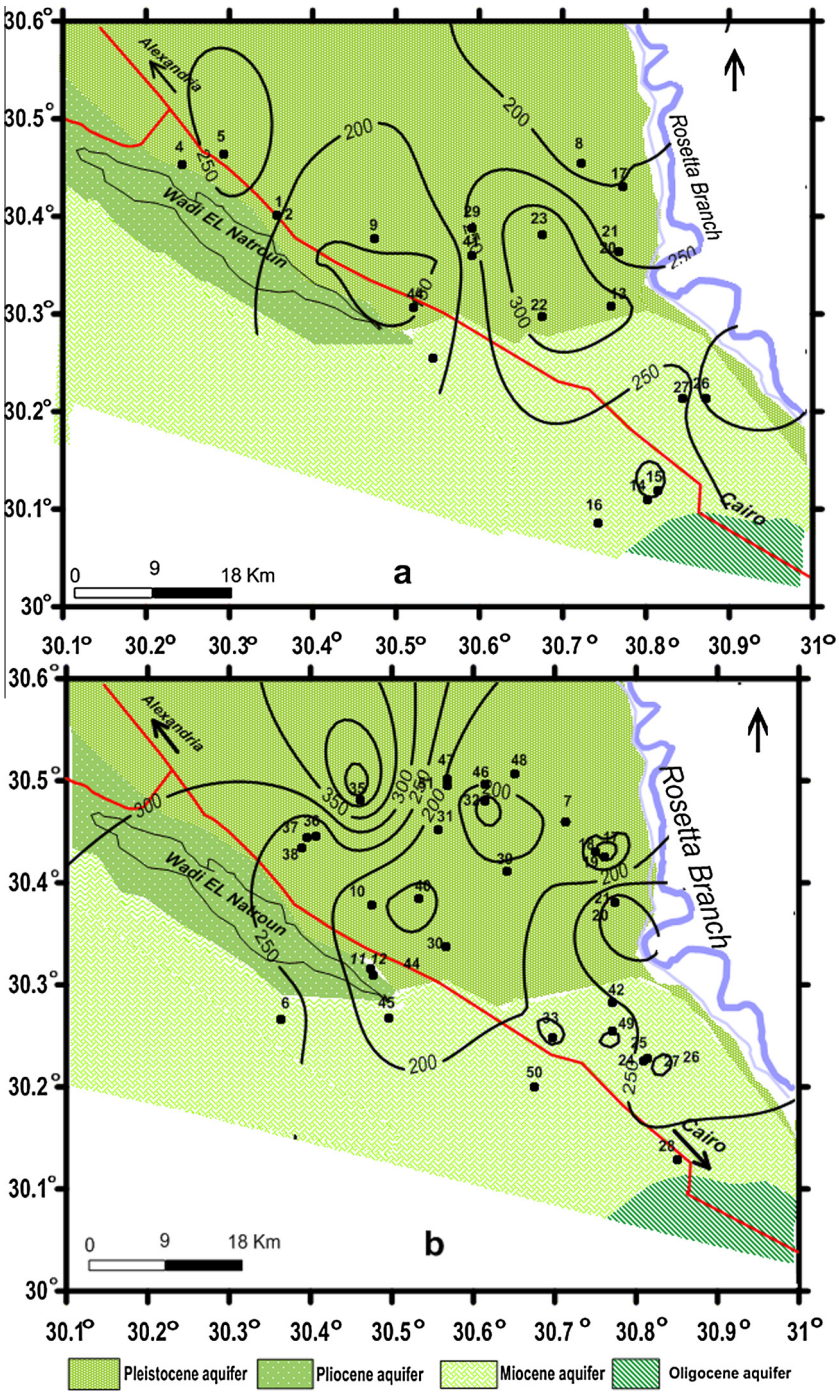

Figure 14 Iso-bicarbonate contour map of the shallow groundwater (a) and the deep groundwater (b).

shallow and deep groundwater, but in general it increases to the east.

Nitrate concentrations range from 0 to 120 mg/l with an average of 8 mg/l (Table 1). The iso-concentration nitrate maps (Fig. 15a and b) in the Quaternary aquifer indicate a marked increase in the nitrate ion toward the eastern part of study area where the large-scale irrigation and intensive use of fertilizers as well as the existence of the oxidation bonds of the sewage water of Sadat City. The concentration of nitrate in shallow zone is much higher than that of the deeper zone. Nitrate content in the Miocene aquifer is much lower than that of the Quaternary aquifer and its increasing trend is also to the east where much application of fertilizers.

5.2. *Hydrochemical classification*

The semi-logarithmic method proposed by Scholler (1962) can be used to provide quick visual comparison of different water chemical analyses. Using Schoeller diagram five main

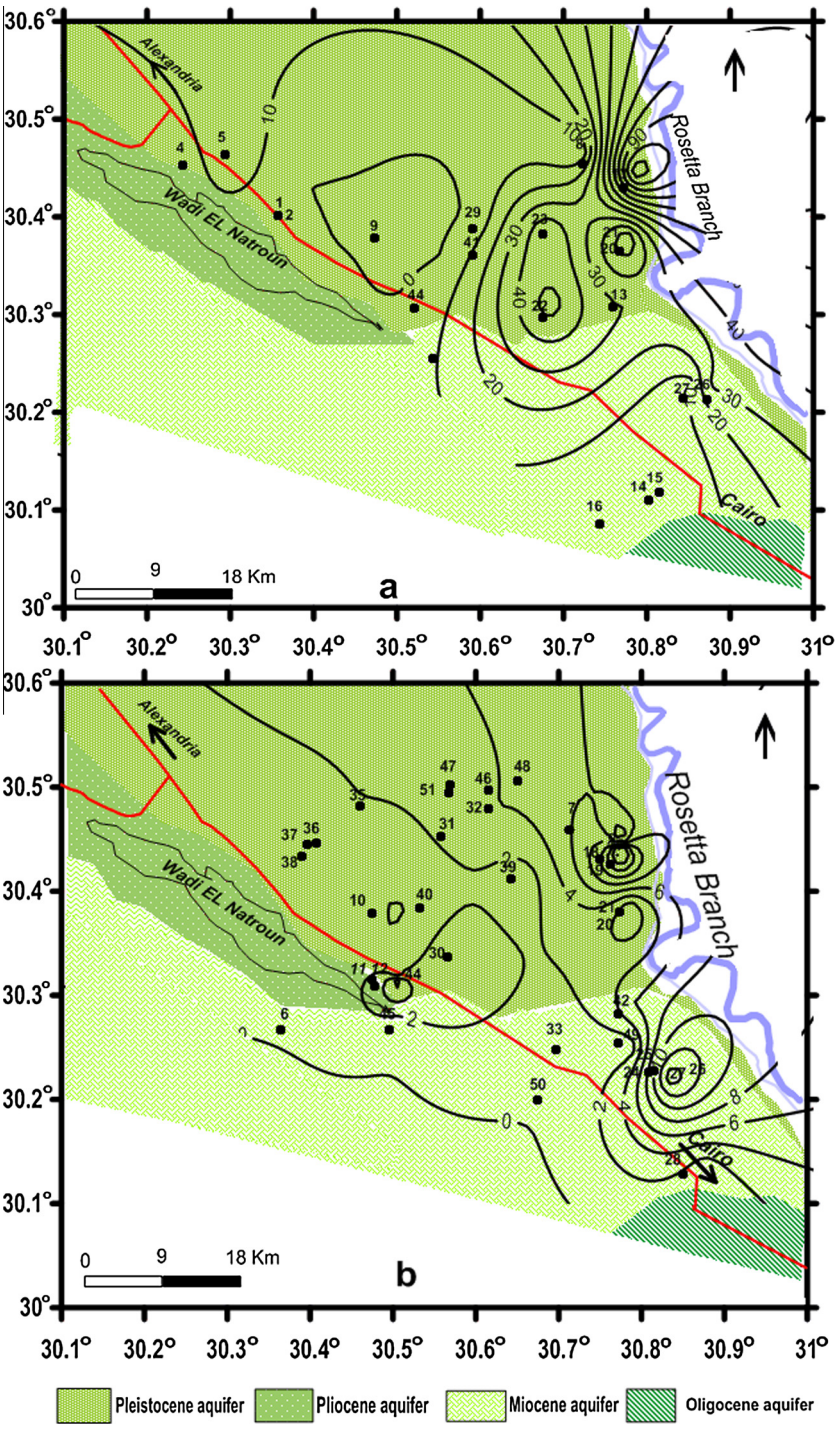

Figure 15 Iso-nitrate contour maps of the shallow groundwater (a) and the deep groundwater (b) in the study.

categories of groundwater types can be recognized as shown in Fig. 16a and b.

1. Na–Cl water type. This type of water appears nearly on most of the samples because chloride ion is dominant in the western part of the area where the water is more deeper compared to the eastern part and represents the end of the water path.
2. Na–HCO_3 water type. It is mostly represented in the deep groundwater just close to the NaCl type. This phenomenon reflects the exchange processes due to the interaction between the carbonate rich groundwater and NaCl water type.
3. Mg–Cl water type. It is more common in the southern part of the area and indicates a kind of exchange between NaCl water and Mg-rich minerals in the aquifer.

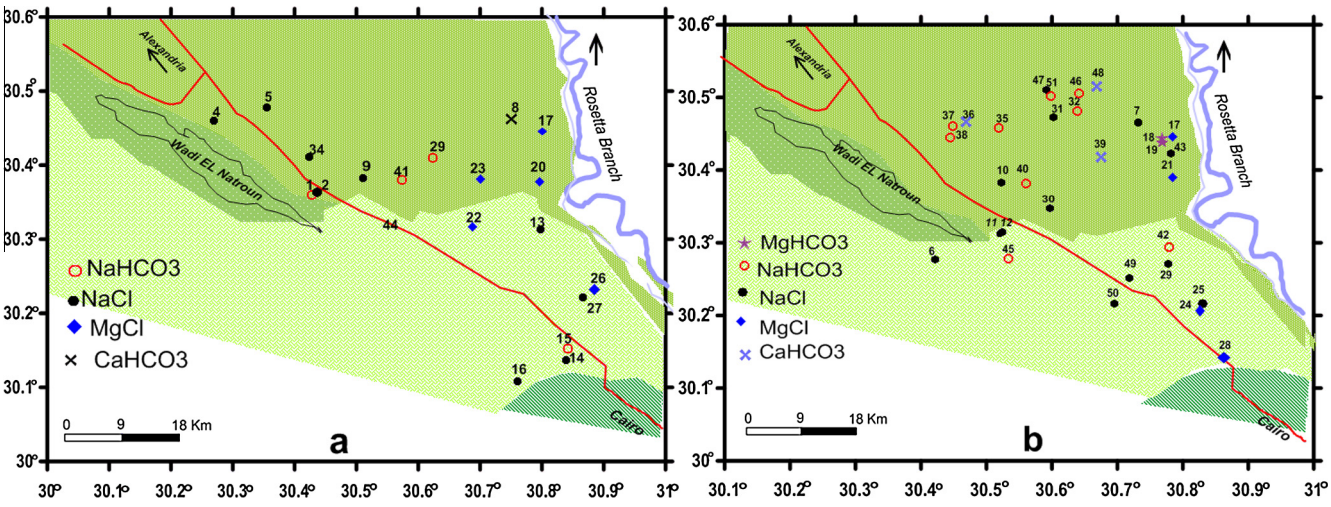

Figure 16 Spatial distribution of the chemical water types in shallow zones (a) and the deep zones (b).

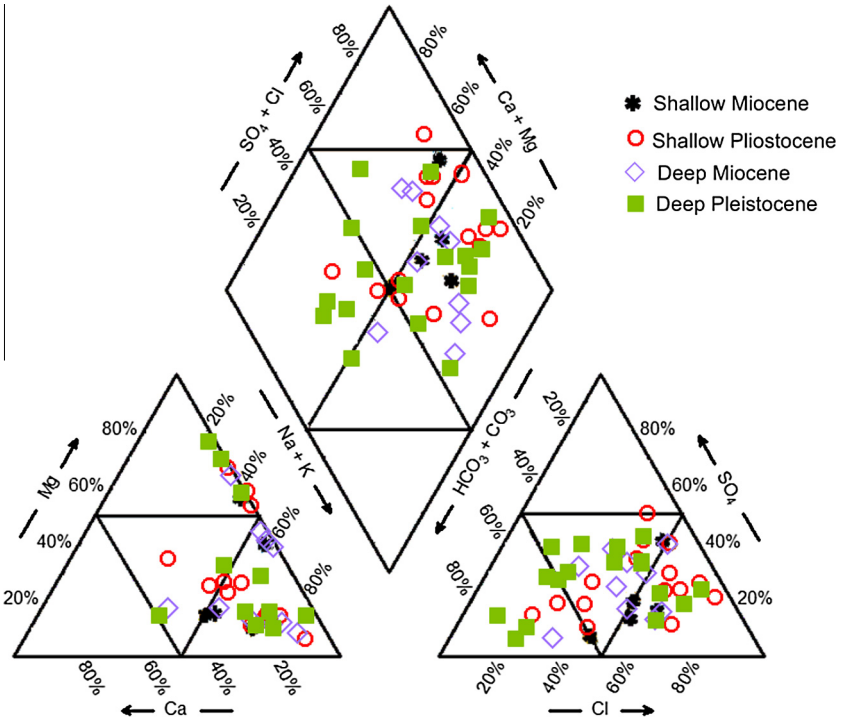

Figure 17 Hydrochemical classification of the groundwater samples by applying Piper diagram.

4. Ca–HCO_3 water type. The spatial distribution reveals that Ca $(HCO_3)_2$ type is not common type.
5. Mg–HCO_3 water type. The areal distribution of this chemical water type indicates that, Ca $(HCO_3)_2$ and Mg $(HCO_3)_2$ are associated with the deeper groundwater to the east more than the shallower zones.

The areal distribution of the water chemical type, (Fig. 16), indicates that, the groundwater of the Pleistocene and Miocene aquifers is characterized by the dominating of the sodium chloride/bicarbonate types while the other types of waters have limited appearance. Such combinations between these two chemical types indicate the predominance of ion exchange processes and water–rock interaction.

The distribution of the samples points on the Piper diagram (Fig. 17) highlights that, the samples are highly deviated toward the field of Mg + Na domination and away from the field of Ca, that composition characterizes the advanced mineralization stages. The distribution is more or less identical between the zone of Cl and that of CO_3 + HCO_3 domination. Ca + Mg are companied with either CO_3 + HCO_3 or SO_4 + Cl indicating the fresh water changed to mineralized water due to addition of SO_4 and Cl from soils or evaporation processes. Shifting of the samples from pure Na Cl water type to the addition of HCO_3 represents the exchange processes.

Sulin's diagram (1946) is used for determining the origin of the groundwater, either marine, or meteoric. According to Sulin diagram, (Fig. 18), three water types are recognized in

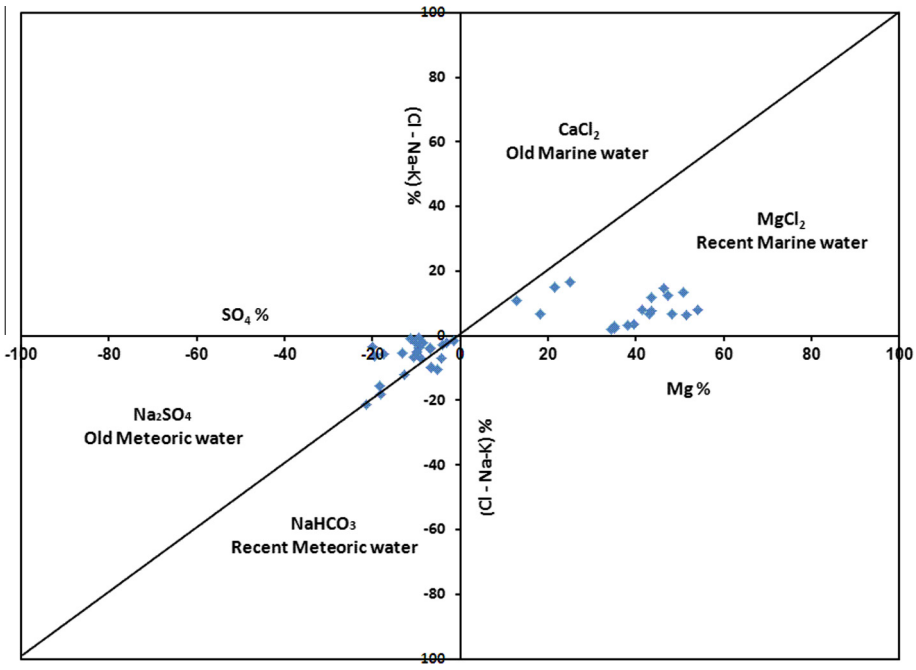

Figure 18 Genetic types of groundwater by applying Sulin's diagram.

the studied groundwater $MgCl_2$, Na_2SO_4 and $NaHCO_3$. Most of the water samples are of old meteoric origin (Na_2SO_4) and old marine origin ($MgCl_2$ type). $MgCl_2$ does not indicate water of marine origin but it reveals that the dissolution of marine salts from the host rocks is a predominant process. A few samples are of the carbonate type ($NaHCO_3$) which is of recent meteoric origin.

5.3. Cluster analysis

Cluster analysis is a useful way of objectively organizing a large data-set into groups on the basis of a given set of characteristics. This can ultimately assist in the recognition of potentially meaningful patterns (Swanson et al., 2001). Hydrochemical results of all samples were divided into four principal water groups based on major ions and each group has distinguished chemical characteristics (Fig. 19). The areal distribution of each group is shown in Fig. 20a and b and the average chemical compositions are listed in Table 2. The first group (1) characterizes the shallow groundwater in the study area. This group has the highest TDS average (2322.5 ppm) and the ionic order is Na > Ca > Mg and Cl > SO_4 > HCO_3. Group (2) samples have average TDS value equals 1734 ppm, and the ionic order is Na > Mg > Ca and SO_4 > Cl. These samples are located in the east of the study area in both shallow and deep zones where higher Mg concentrations are recorded. Water samples of group (3) have relatively low TDS (750.1 ppm) and are dominated by Na > Ca and HCO_3 > Cl ionic orders. These samples are mostly located in the deep zone more than shallow zone. Group (4) samples have the lowest average TDS value (384.7 ppm), and are dominated by Na > Ca and HCO_3 > Cl water. It is similar to group (3) but with lower concentration percentages of ions. These samples are also predominating in the deep zone compared to the shallow zone.

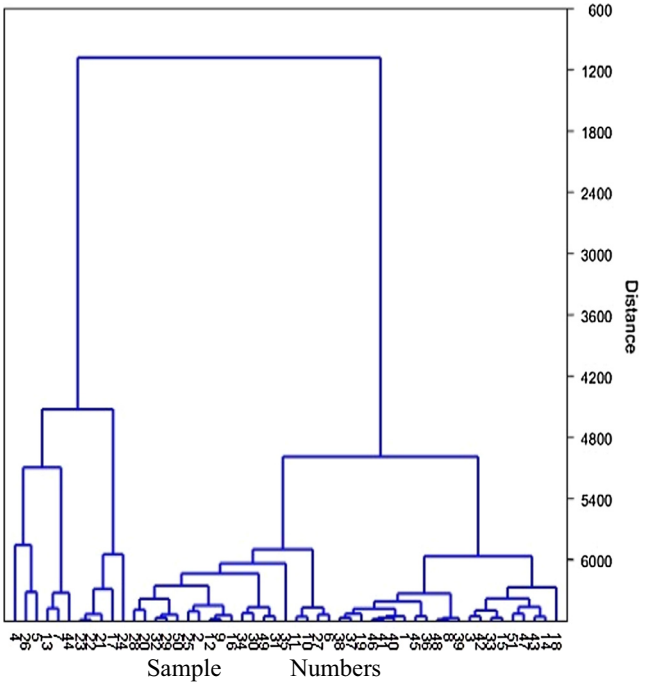

Figure 19 Cluster analysis for the water samples in the study area.

The dendograms for classifying the ions association in the studied groundwater are shown in Fig. 21. The recognized chemical groups in the shallow groundwater system are Na–Cl–Mg–SO_4 and NO_3–K–HCO_3–Ca (Fig. 21a). The deep groundwater system shows different ions associations which are NO_3–K, SO_4–HCO_3–Ca–Mg and Cl–Na (Fig. 21b). The abundance of Na–Cl in both zones could be related to

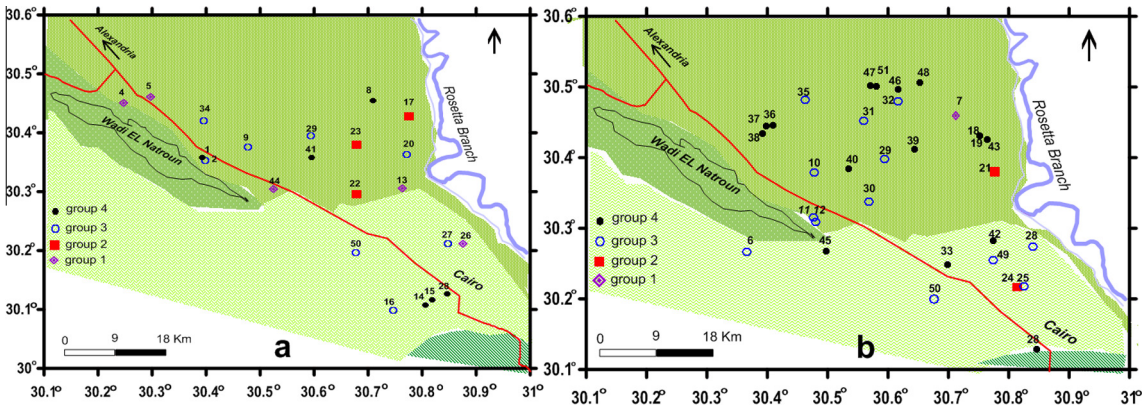

Figure 20 The spatial distribution of Cluster's groups in shallow zone (a) and in deep zone (b).

dissolution of halite as well as the evaporation effect. Mg–SO_4 association accompanied with Na–Cl in the shallow zone indicates the dissolution of marine salts. Presence of NO_3–K association in the shallow and the deep zones indicates the surface infiltration where the use of fertilizers in the agricultural activities. Ca–HCO_3 association accompanied with NO_3–K in the shallow groundwater reflects the formation of the dissolved calcite by atmospheric CO_2 and organic matter in the soil zone. The predominance of the water–rock interaction processes in the deep zone is reflected by Mg–Ca–HCO_3–SO_4 association where the ion-exchange and the chemical weathering may occur.

5.4. Mechanisms controlling waters chemistry

Gibbs diagram represents the ratio of Na/(Na + Ca) and Cl/(Cl + HCO_3) as a function of TDS which is widely used to assess the functional sources of dissolved chemical constituents (Gibbs, 1970) such as, precipitation dominance, rock dominance and evaporation dominance. The chemical data of the groundwater samples from the study area are plotted in Gibb's diagram (Fig. 22). Evaporation is the major process affecting the source of cations content in the present groundwater (Fig. 22a), while, rock dominance is the major process affecting the source of anion content in the present groundwater (Fig. 22b). To detect the ion exchange process, the relationship between the excess of (Ca + Mg) from the equation [(Ca + Mg) – (SO_4 + HCO_3)] and the excess of Na from the equation (Na–Cl), was plotted as in Fig. 23. Most of the plotted samples have excess of Na which could be derived from replacing Ca + Mg indicating ion exchange process. Some samples have excess of both (Ca + Mg) and Na which reveals a water–rock interaction without any exchange processes.

5.5. Groundwater quality

The U.S. Salinity Laboratory Staff Classification (Fig. 24) indicates that most of the studied groundwater samples have low SAR and medium to high salinity content. Samples located in the field C2S1 are satisfactory for plants having medium salt tolerance on almost all soils; irrigation by this water requires a moderate amount of leaching. Class C3S1 samples are characterized by high salinity, low sodium hazard and satisfactory for plants having moderate salt tolerance on soil of moderate to good permeability (moderate leaching), and irrigation by this water requires regular leaching and special management. The former two classes are represented in both Quaternary and Miocene aquifers. Some water samples from the Quaternary aquifer deviated toward very high salinity and medium to high SAR (C4S2 and C4S3, respectively). Generally this water types are not suitable for irrigation under ordinary conditions, but it may be used occasionally under special conditions.

Table 2 Statistical classification of the groundwater samples into four groups based on chemical composition.

	Group 1			Group 2			Group 3			Group 4		
	Average	Max	Min	Average	Max	Min	Average	Max	Min	Average	Max	Min
TDS	2322.5	3123	1728	1734	1954	1280	750.1	921	567	384.7	550	220
Ca	120.5	150	28	13.6	21	10	41.8	70	9	37.3	195.2	7
Na	518	794	308	266.2	290	215	167.8	238.1	40	69.4	138	20
Mg	109.6	361.4	38.7	215.588	251.3	130.6	25.6	112	7.28	27.6	139	7.3
K	18.3	35.6	11	59.738	72.5	32.5	9.6	25	3	8.3	37	3
HCO_3	251.5	341.1	140.8	311.2	350	204	222.1	494	153	170.5	259.1	6
Cl	777.9	1220	584.9	386.96	440	329	205	310	112	64.1	185	0
SO_4	483.2	784	283.7	500.52	570	281.6	128.2	219	52.6	60.5	183	5.7
NO_3	14.8	30.4	0.85	47.82	120	0	1.9	7.6	0	7.7	55	0.07
Sample no.	4 5 7 13 26 44			11 21 22 23 24			28 20 32 29 50 25 2 12 9 16 34 30 49 31 31 35 11 10 27 6			38 37 19 46 41 40 1 45 36 48 8 39 3 42 33 15 51 47 43 14 18		

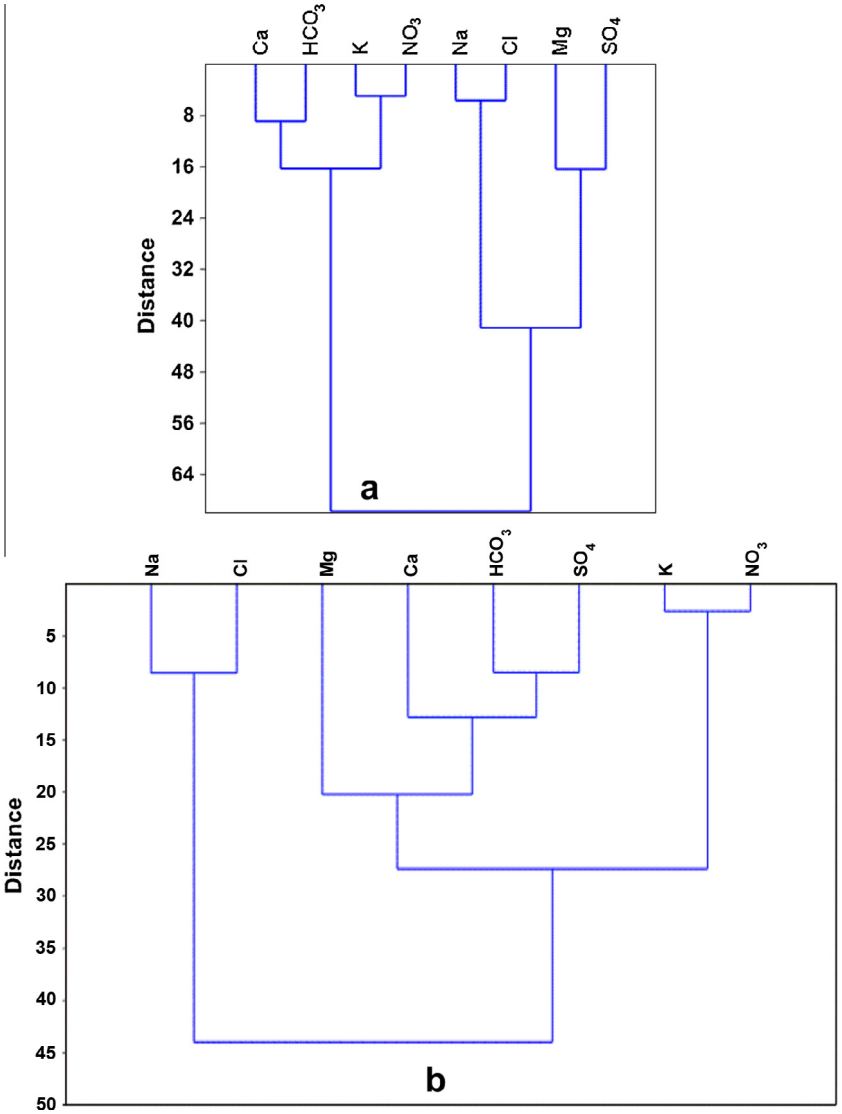

Figure 21 The ion associations in the shallow (a) and the deep (b) groundwaters.

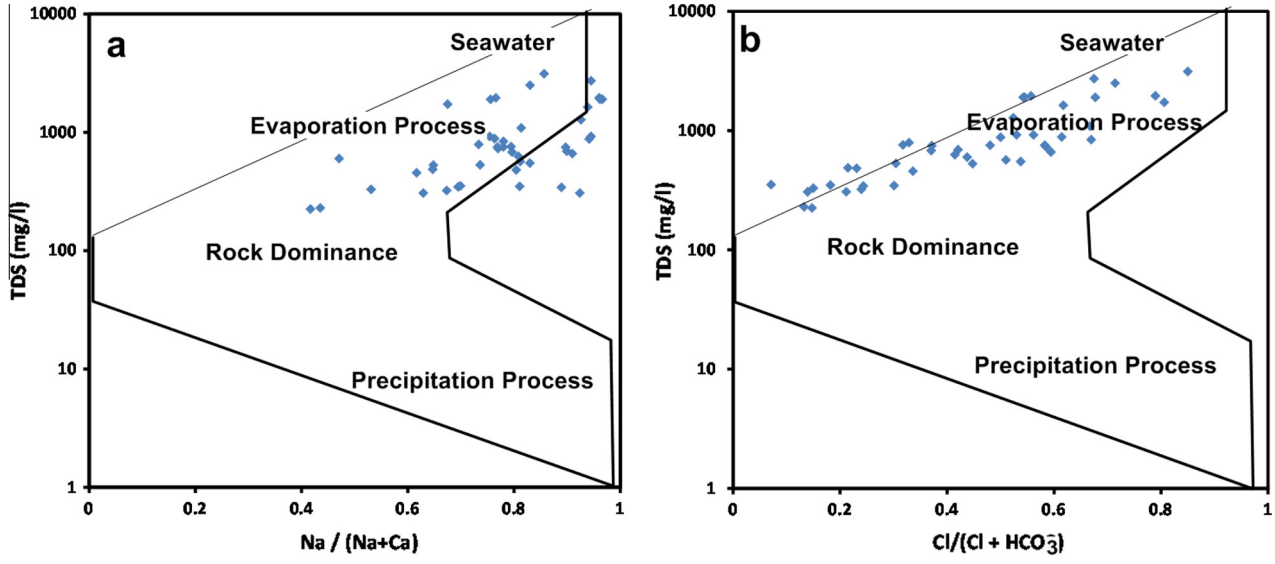

Figure 22 Diagrammatic representation of the processes controlling the chemistry of the studied groundwater.

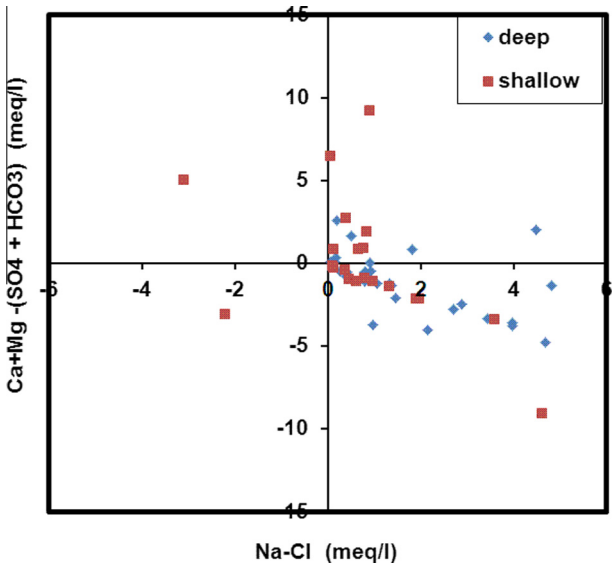

Figure 23 The relationship between [Ca + Mg–SO_4–HCO_3] and [Na–C1].

6. Discussion and conclusions

The studied groundwater flows from the east and north directions where the surface water sources are located to the west and south directions. Wadi El-Natrun is a natural discharge area for the groundwater and the hydraulic gradient increases gradually from east to west which could be related to topographic and fault effects. Water table change between 1960 and 2010 showed a drawdown of groundwater levels reached about 25 m mainly in the southern part of the region. Seepage from the irrigation channel and excess uses of surface irrigation water at the northern part of the area lead to water level rise about 5 m to the east and 10 m to the west. In the southern part, to avoid wells drying and aquifer depletion, it is recommended to regulate the pumping rate of the current wells and construct surface channel network to minimize groundwater pumping.

Electric logs were used to estimate resistivity of water, total porosity, effective porosity, formation factor and, permeability. The formation water resistivity (R_w) averages 15.2 ohm m. The formation factor (F) averages 5.1 and total porosity has an average of 36.5%, while the effective porosity has an average of 33.1%. The average permeability of the aquifers is 1126.3 mdarcy. In addition, the gamma ray logs are used to estimate volume share of shale and showed that the average value reached about 34.6%. The recharge area located to the northwestern direction has higher values of porosity, effective porosity and permeability. On the other hand, the recharge area has lower values of volume share of shale. This phenomenon helps in increasing the infiltration from the irrigation channels.

Geochemical investigation of the groundwater in the study area has indicated that there is a gradual increase in water salinity toward the east and northwest directions in shallow wells and toward the east in the deep wells in both aquifers. However, the shallow groundwater of the two aquifers has higher TDS than the deeper one. The areal distribution of the major ions in the shallow zones of the Pleistocene aquifer indicated that there is a gradual decrease of the major ion contents in the eastern and southern part except Mg content which increases to the central and eastern parts. In deeper zone, the concentration of ions increases toward west and northwest. Generally, the major ion content in the shallow zones is higher than that of the deep zones, except Mg due to soil effect and evaporation processes.

Comparing the hydrochemical classification with the groundwater flow system was useful for detecting the

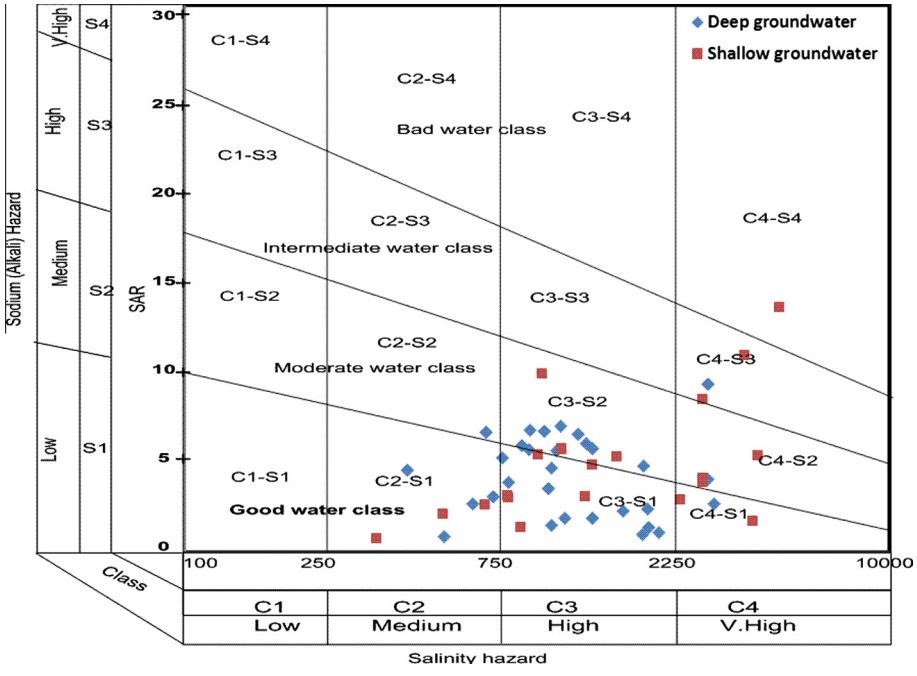

Figure 24 US salinity laboratory stuff diagram for classification of the studied groundwater for irrigation purposes.

hydro-geochemical change along the flow path. Na–Cl type is recorded in the western parts at the end of the flow path where Na–HCO_3 water type is dominant in the deeper zone east to the NaCl type. Such arrangement reveals that the ion exchange process between the groundwater and the country rocks has been occurred to form the $NaHCO_3$ type and losing the HCO_3 along the flow path to form NaCl type.

Statistical classification was quite useful in the present groundwater according to salinity, associations of dissolved elements, geographical location as well as sample depth. Three groups were recognized, the first group (1) characterizes the shallow groundwater in the study area where it has the highest TDS average (2322.5 ppm) and the ionic order is Na > Ca > Mg and Cl > SO_4 > HCO_3. Group (2) samples are located to the east of the study area in both shallow and deep zones and have average TDS value equals 1734 ppm, and the ionic order is Na > Mg > Ca and SO_4 > Cl. Water samples of group (3) mostly characterize the deep samples, have relatively low TDS (750.1 ppm) and are dominated by Na > Ca and HCO_3 > Cl ionic orders. Group (4) samples are also predominating in the deep zone and have the lowest average TDS value (384.7 ppm) with the same ionic order of group (3). The recognized chemical groups in the shallow groundwater system are Na–Cl–Mg–SO_4 and NO_3–K–HCO_3–Ca (Fig. 21a). The deep groundwater system shows different ions associations which are NO_3–K, SO_4–HCO_3–Ca–Mg and Cl–Na. The ion groups of the shallow groundwater reflect the impact of the soil chemical process, agricultural activities and the dissolution of the marine deposits. The ion associations of the deep groundwater indicate the water rock interaction and mineral weathering.

Three water types were recognized in Sulin's diagram, $MgCl_2$, Na_2SO_4 and $NaHCO_3$. Most of the water samples are of old meteoric origin (Na_2SO_4) and old marine origin ($MgCl_2$ type) and a few samples are of recent meteoric origin ($NaHCO_3$ type). $MgCl_2$ type does not related to marine water origin but its salts are derived from the dissolution of the marine salts of the country rocks. This could be supported by Gibbs diagram results where evaporation and rock dominance are both dominant in the present groundwater. The ion exchange reaction is a dominant process in both shallow and deep groundwater and it is detected using the plot of Ca + Mg–SO_4–HCO_3 vs Na–Cl where Na replaces both Ca and Mg. Based on the values of SAR, and EC in the studied groundwater, most of the groundwater samples are suitable for irrigation uses except for some samples in both shallow and deep zones which have higher EC values.

Acknowledgments

The data used in this research are a part from the M.Sc. thesis of the second author; therefore, Abdel-Monem T. abdel-Hameed and Taher M. Hassan are thanked for permitting the publishing of this work as they and the first author were supervising the thesis. The authors are thankful to Tanta University, Egypt, for the financial support during the field and the laboratory work. We thank the two reviewers and the editor for their constructive remarks.

References

Abdel Baki, A.A., 1983. Hydrogeological and hydrogeochemical studies in the area west of Rosetta branch and south of El Nasr canal. Ph.D. Thesis, Fac. Sci., Ain Shams University.

Ahmed, S.A., 1999. Hydrogeological and Isotope Assessment of Groundwater in Wadi El-Natrun and Sadat City, Egypt. Department of Geology, Faculty of Science, Ain Shams University, Cairo, Egypt.

Ahmed, M.A., Samie, S.G., El-Maghrabi, H.M., 2010. Recharge and contamination sources of shallow and deep groundwater of pleistocene aquifer in El-Sadat Industrial City: isotope and hydrochemical approaches. Environ. Earth Sci. 62 (4), 751–768. http://dx.doi.org/10.1007/s12665-010-0563-.

Archie, G.E., 1942. The electrical resistivity log as an aid in determining some reservoir characteristics. T. Am. I. Min. Met. Eng. 146, 54–62.

El-Gamal, H., 2005. Environmental Tracers in Groundwater as Tools to Study Hydrological Questions in Arid Regions. Ruperto-Carola University of Heidelberg, Germany, p. 146.

El Ghazawi, M.M., Atwa, S.M., 1994. Contributions of some structural elements to the groundwater conditions in the southwestern portion of the Nile Delta. Geol. Soc. Egypt, Cairo, Egypt 38 (2), 649–667.

Gibbs, R.J., 1970. Mechanisms controlling world water chemistry. Science 170, 1088–1090.

Guyod, H., 1966. Interpretation of electric and gamma ray logs in water wells. SPWLA 6 (5), 29–44.

Hiscock, K.M., 2005. Hydrogeology; Principles and Practice. Blackwell Publishing Company, p. 389.

Ibrahim, S., 2005. Groundwater Resources Management in Wadi El-Farigh Area and Its Vicinities for Sustainable Agricultural Development. Faculty of Engineering, Ain Shams University, Cairo, Egypt.

Jorgensen, D.G., 1988. Estimating permeability in water-saturated formations. SPWLA 29, 401–409.

Jorgensen, D.G., 1989. Using geophysical logs to estimate porosity, water resistivity and intrinsic permeability. US geological Survey Water Supply, paper 2321, 24p.

Said, R., 1962. The Geology of Egypt. Elsevier CO., Amsterdam, New York, p. 380.

Schlumberger, 1972. Log Interpretation Volume 1 – Principles.

Scholler, H., 1962. Geochemie des eaux souterraines Rev. de l'institut francais du petrole, vol. 10. pp. 230–244.

Sulin, V.A., 1946. Waters of Petroleum Formations in the System of Natural Water. Gostoptekhiz-dat, Moscow (in Russian). pp. 35–96.

Swanson, S., Bahr, J., Schwar, M., Potter, K., 2001. Two-way cluster analysis of geochemical data to constrain spring source waters. Chem. Geol. 179, 73–91.

U.S. Salinity Laboratory Staff, 1954. Diagnosis and Improvement of Saline and Alkaline Soils. U.S Dept. of Agric., Handbook, 60, Washington, D.C., p. 160.

Winslow, A.G., Kister, L.R., 1956, Saline-Water Resources of Texas: U.S. Geological Survey Water-Supply Paper 1365, p. 105.